Available online at www.sciencedirect.com
ScienceDirect
Journal of Computational Physics 227 (2008) 3322–3357
JOURNAL OF COMPUTATIONAL PHYSICS
www.elsevier.com/locate/jcp

High-order local absorbing conditions for the wave equation: Extensions and improvements

Thomas Hagstrom [a], Assaf Mar-Or [b], Dan Givoli [c,*]

[a] *Department of Mathematics and Statistics, The University of New Mexico, Albuquerque, NM 87131, USA*
[b] *Inter-Departmental Program for Applied Mathematics, Technion – Israel Institute of Technology, Haifa 32000, Israel*
[c] *Department of Aerospace Engineering, Technion – Israel Institute of Technology, Haifa 32000, Israel*

Received 9 June 2007; received in revised form 22 November 2007; accepted 27 November 2007
Available online 8 December 2007

Abstract

The solution of the time-dependent wave equation in an unbounded domain is considered. An artificial boundary $\mathcal{B}$ is introduced which encloses a finite computational domain. On $\mathcal{B}$ an absorbing boundary condition (ABC) is imposed. A formulation of local high-order ABCs recently proposed by Hagstrom and Warburton and based on a modification of the Higdon ABCs, is further developed and extended in a number of ways. First, the ABC is analyzed in new ways and important information is extracted from this analysis. Second, The ABCs are extended to the case of a *dispersive medium*, for which the Klein–Gordon wave equation governs. Third, the case of a *stratified medium* is considered and the way to apply the ABCs to this case is explained. Fourth, the ABCs are extended to take into account *evanescent modes* in the exact solution. The analysis is applied throughout this paper to two-dimensional wave guides. Two numerical algorithms incorporating these ABCs are considered: a standard semi-discrete finite element formulation in space followed by time-stepping, and a high-order finite difference discretization in space and time. Numerical examples are provided to demonstrate the performance of the extended ABCs using these two methods.

Keywords: Waves; High-order; Artificial boundary; Absorbing boundary condition; Higdon; Auxiliary variables; Finite elements; Finite differences; Wave guide; Dispersive waves; Stratified medium; Evanescent waves

1. Introduction

With the improvement of computational methods for the solution of wave problems in unbounded media, as encountered in geophysics, weather prediction, underwater acoustics, aeroacoustics, etc., the need for and interest in accurate schemes for treating artificial boundaries has increased in recent years. Among these

* Corresponding author. Tel.: +1 972 829 3814; fax: +1 972 829 2030.
E-mail addresses: hagstrom@math.unm.edu (T. Hagstrom), pierrot@technion.ac.il (A. Mar-Or), givolid@aerodyne.technion.ac.il (D. Givoli).

0021-9991/$ - see front matter © 2007 Elsevier Inc. All rights reserved.
doi:10.1016/j.jcp.2007.11.040

methods, two have emerged as especially powerful [1]. The first one is the perfectly matched layer (PML) method, devised by Bérenger [2] in 1994 and since then further developed and used by many authors (see also [3]). The second type of method is that of high-order absorbing boundary conditions (ABCs). The use of ABCs has been very popular since the early 1970s – see the survey in [4] – but the recent development referred to here is the ability to use ABCs of an *arbitrarily high order*. The first such ABC has been devised by Collino [5] in 1993, and a few other formulations followed; see a survey in [6].

ABCs are boundary conditions imposed on artificial boundaries of computational domains. Given a wave problem in an unbounded medium, the infinite domain is truncated via an artificial boundary $\mathcal{B}$, thus dividing it into a finite computational domain Ω and a residual infinite domain D. A special boundary condition, called an ABC, is imposed on $\mathcal{B}$ in order to complete the statement of the problem in Ω (i.e. make the solution in Ω unique) and to ensure that no (or little) spurious wave reflection occurs from $\mathcal{B}$. The problem is then solved numerically in Ω. The setup is illustrated in Fig. 1 for a two-dimensional semi-infinite wave-guide. In this setup, which will serve as a prototype for this paper, $\mathcal{B} = \Gamma_{\mathrm{E}}$ is a cross-section of the wave-guide which constitutes the east side of Ω.

In theory, some of the classical ABCs, such as the Engquist-Majda ABCs [7] or the Bayliss–Turkel ABCs [8] can be defined up to any desired order. However, the appearance of increasingly high order derivatives in these ABCs renders them impractical beyond a certain order, typically 2 or 3. For example, the P-order Higdon ABC [9,10] involves P-order derivatives in space and time, and is thus very inconvenient for implementation when P is large. In fact, discrete Higdon conditions were developed in the literature, with the exception of [11], up to third order only.

There are two ways to construct practical ABCs with arbitrarily *high order* accuracy. The first way is to use an ABC based on a *nonlocal* operator; examples include the early work of Fix and Marin [12] and the Dirichlet-to-Neumann ABC [13], both in the frequency domain. However, in the time-domain nonlocal ABCs nonlocal conditions also require time convolutions. Although these can be treated efficiently in many cases [14], the nonlocal methods are inflexible in terms of the computational domain (e.g. rectangular boundaries cannot be used) and the governing equations (e.g. such methods are unavailable for stratified media.) The second type of high-order ABCs are those which make use of special *auxiliary variables*. The latter eliminate the need for any high-order derivatives; thus these ABCs can be practically employed with an arbitrarily high order [6,15]. One example is the high-order ABC of Hagstrom and Hariharan [16] for circular and spherical boundaries. Givoli and Neta [17,18] reformulated the Higdon ABC (in Cartesian coordinates) as a high-order ABC. Later, Hagstrom and Warburton [19] proposed a modification to the Givoli–Neta formulation with enhanced stability. The Hagstrom–Warburton (H–W) formulation is the basis for the present paper.

In [20] we compare the H–W formulation with the Givoli–Neta formulation from various aspects, and apply the former to exterior wave problems in two dimensions using a finite element scheme. In doing this we have to use special corner conditions at the four corners of the artificial boundaries. In [21] we concentrate on the question of choosing the computational parameters $0 < a_j \leqslant 1$, for $j = 0, 1, \ldots P$, which appear in the P-order H–W ABC and which signify cosines of incidence angles. A point of emphasis in [21] is that a comparison of boundary conditions based solely on the magnitude of reflection coefficients for propagating modes is a poor predictor of actual performance, particularly as the order is increased. This fact has been noted before, for example by Taflove and Hagness [22, Chapter 6]. In this reference it is suggested that the cause is wave speed mismatch resulting from discretization error. However, the highly-resolved calculations per-

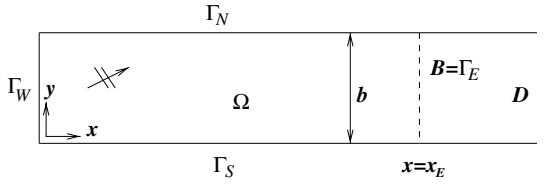

Fig. 1. A semi-infinite wave-guide, with an artificial boundary $\mathcal{B} = \Gamma_{\mathrm{E}}$ on which an ABC is to be applied.

formed in [21] effectively rule out this explanation. In fact, the exact error analysis presented by Diaz and Joly [23] recommends the choice $a_j = 1$ for all j. In [21] we find that this choice is satisfactory in general, although not necessarily optimal. In addition, we present and test an adaptive scheme which controls the time-varying values of P and the a_j.

In the present paper we consider the H–W formulation in a two-dimensional wave guide, as in Fig. 1. Thus we avoid the issue of corner conditions, which is outside the scope of this paper. In most of our developments we make the simple choice of parameters $a_j = 1$, following the general conclusions of [21]. This choice is shown to be acceptable for moderate solution times and accuracy requirements, though for more challenging examples we use the evanescent mode corrections introduced below.

There has been much discussion in the literature concerning the relative merits of ABC and PML (see e.g. [22, Chapter 7] and [24, Chapter 7]). However, as was first shown by Asvadurov et al. in [25], the methods are in fact deeply connected. As we will mention below, the H–W formulation used here can be interpreted as a particular semi-discretization of a PML. Exact error analysis presented in [26] does indicate that the long time behavior of standard PML formulations is better than that of standard ABCs. However, the inclusion of evanescent mode corrections removes this difficulty, leading to optimal long time error estimates [27,28]. Of course the actual performance of any method will depend on the details of the discretization. We will show below that even for marginally resolved discretizations using standard linear finite elements we can achieve an accuracy which is on average as good as can be obtained with an extended domain calculation.

The purpose of this paper is to further develop and extend the H–W ABCs in various ways. Since it is desired that these ABCs eventually become a practical and powerful tool in the solution of realistic problems in fields like geophysics, weather prediction, aeroacoustics, etc., it is very important to make them applicable and verify their good performance for the widest possible range of configurations. Admittedly, the basic governing equation used in this paper (the Klein–Gordon equation, or as a special case the standard wave equation) is relatively simple, and it would be interesting and important to check how the proposed ideas are carried over to more involved problems such as those governed by the shallow water equations, Maxwell's equations and the linearized Euler equations. However, we feel that before attacking these more complicated problems it is essential to validate the new techniques developed here by applying them to a simple class of problems that would still highlight all the basic numerical phenomena involved, and would give a good evaluation of the method performance.

We discuss the incorporation of the extended ABCs in two different numerical schemes. The first is a finite element formulation using bilinear elements in space and a Newmark (2nd-order accurate) scheme in time, which is implemented slightly differently than in [20]. The second is based on a high-order finite difference discretization in space and time, and yields much more accurate results. Despite the higher accuracy of the latter, we feel that it is important to include the FE formulation and results here, for two reasons. First, the superiority of the FD scheme originates only from the fact that the FD stencil used is high-order in space and time, whereas the FE scheme chosen is the most standard one, hence low order in space and time. Of course, replacing the standard FE scheme by a high-order FE method (p-version or spectral elements) is bound to eliminate this limitation in accuracy. Second, FE codes are very commonly used in various fields of application, and we would like to enable one to incorporate the ABC proposed here in an existing FE code.

After recalling the basic H–W formulation (Section 2), we derive the algebraic ABC equations obtained for the basic wave-guide modes (which are identical to the plane wave equations in the exterior case), solve these equations analytically, and extract important information from the solution (Section 3). Then we calculate the error associated with the P-order ABC operator with respect to the exact boundary operator (Section 4). We show how the ABCs can be extended for a dispersive medium, where the Klein–Gordon wave equation governs (Section 5), for a stratified medium (Section 6) and for the case where evanescent modes (and not only propagating modes) are taken into account by the ABC (Section 7). We discuss the incorporation of the extended ABCs in the two different numerical schemes mentioned above (Section 8). We present some numerical examples using these two schemes to demonstrate the performance of the extended ABCs (Section 9). We end the paper with some concluding remarks (Section 10).

2. The basic formulation

We consider waves propagating in a two-dimensional guide of width b as described in Fig. 1. A Cartesian coordinate system (x, y) is introduced such that the longitudinal direction of the guide is the x direction. In the guide we consider the linear inhomogeneous scalar wave equation,

$$\partial_t^2 u - c^2 \nabla^2 u = s. \tag{1}$$

Here and elsewhere we use

$$\partial_a^i = \frac{\partial^i}{\partial a^i} \tag{2}$$

as a shorthand for partial derivatives. In (1), u is the unknown wave field, c is the given wave speed, and s is a given wave source function. It is assumed that outside a compact region, where the speed c and the wave source s may be general, c is constant and s vanishes. On the south, north and west boundaries Γ_S, Γ_N and Γ_W some boundary conditions are specified. To fix ideas we shall assume the conditions,

$$u = u_W \quad \text{on } \Gamma_W, \tag{3}$$

$$\partial_y u = 0 \quad \text{on } \Gamma_S \text{ and } \Gamma_N. \tag{4}$$

Here u_W is a given function on Γ_W. To complete the statement of the problem, the initial conditions

$$u(x, y, 0) = u_0, \quad \partial_t u(x, y, 0) = v_0, \tag{5}$$

are given at time $t = 0$ in the entire domain. We assume that the functions u_0 and v_0 have a local support.

We now truncate the semi-infinite domain by introducing an artificial east boundary $\mathcal{B} \equiv \Gamma_E$, located at $x = x_E$, $0 \leqslant y \leqslant b$; see Fig. 1. This boundary divides the original semi-infinite domain into two subdomains: an exterior domain D, and a finite computational domain Ω which is bounded by Γ_W, Γ_N, Γ_S and Γ_E. We choose the location of Γ_E such that the entire support of s, u_0 and v_0 and the region of non-uniformity of c are all contained inside Ω. Thus, on Γ_E and in D, the homogeneous counterpart of (1) holds, i.e.

$$\partial_t^2 u - c^2 \nabla^2 u = 0, \tag{6}$$

with a constant coefficient c^2, and the medium is initially at rest.

To obtain a well-posed problem in the finite domain Ω we need to impose a boundary condition on Γ_E. This must be an ABC so as to prevent spurious reflection of waves. We use the H–W ABC [19]. The starting point of this ABC is the recursive relations in the vicinity of Γ_E,

$$(a_0 \partial_t + c\partial_x) u = a_0 \partial_t \phi_1, \tag{7}$$

$$(a_j \partial_t + c\partial_x) \phi_j = (a_j \partial_t - c\partial_x) \phi_{j+1}, \quad j = 1, \ldots, P, \tag{8}$$

$$\phi_{P+1} = 0. \tag{9}$$

Here P is the order of the ABC, the ϕ_j $(j = 1, \ldots P)$ are unknown auxiliary variables defined on the boundary Γ_E, and the a_j are parameters which have to be chosen and which signify (see [19]) cosines of incidence angles.

We make here a few remarks about (7)–(9):

- These recursive relations are a modified version of those defined by Givoli and Neta [17]. The latter, if one eliminates all the auxiliary variables, yield the Higdon boundary operator [9,10]. In [20] we showed the advantage of using the modified recursive relations (7)–(9) over the original ones.
- In our previous papers [19–21] the parameter a_0 appeared on the left side of (7) but not on the right side. Indeed, as long as the medium in D is homogeneous (as we assume in this section) one may replace the a_0 on the right side of (7) by the value 1 without loss of generality. However, later we shall consider inhomogeneous media, where the presence of a_0 on the right side is essential.
- In [21] we discussed the choice of parameters a_j, and proposed an adaptive scheme for dynamically updating them. We showed that the simplest choice $a_j = 1$ is satisfactory in many situations, though we will see below that evanescent mode corrections lead to significant improvements in long-time performance.

The set of conditions (7)–(9) involves only first-order derivatives, even though the order P may be arbitrarily high. However, it cannot serve as an ABC in its present form due to the appearance of the x-derivative in (8), which makes it impossible to discretize the ϕ_j on the boundary Γ_E alone. Therefore we shall manipulate (8) in order to get rid of the x-derivative. It is easy to show, by induction, that each auxiliary function ϕ_j satisfies the wave Eq. (6), i.e.

$$\partial_x^2\phi_j + \partial_y^2\phi_j - \frac{1}{c^2}\partial_t^2\phi_j = 0. \tag{10}$$

We now apply the operator $a_{j-1}(a_j\partial_t + c\partial_x)$ to the jth equation in (8), apply the operator $a_j(a_j\partial_t - c\partial_x)$ to the $j-1$ equation in (8), and add the two resulting equations. This eliminates the mixed-derivative terms $(\partial_{xt}\phi_j)$ and leaves only terms with the 2nd-order derivatives ∂_t^2 and ∂_x^2. Finally we use (10) to eliminate ∂_x^2 and obtain an equation including only the derivatives ∂_t^2 and ∂_y^2 of the auxiliary variables (see below). This equation holds for $j = 2,\ldots,P$. We repeat this process for the case $j = 1$, using the $j = 1$ equation in (8) as well as Eq. (7). Combining all these results gives the complete H–W ABC of order P:

$$(a_0\partial_t + c\partial_x)u = a_0\partial_t\phi_1, \tag{11}$$

$$l_{j,j-1}\partial_t^2\phi_{j-1} + l_{j,j}\partial_t^2\phi_j + l_{j,j+1}\partial_t^2\phi_{j+1} = c^2\left(m_{j,j-1}\partial_y^2\phi_{j-1} + m_{j,j}\partial_y^2\phi_j + m_{j,j+1}\partial_y^2\phi_{j+1}\right), \quad j = 1,\ldots,P, \tag{12}$$

$$\phi_0 \equiv u, \quad \phi_{P+1} = 0, \tag{13}$$

where the coefficients for $j = 1$ are

$$l_{1,0} = 2a_1(1 - a_0^2), \tag{14}$$

$$l_{1,1} = a_0(1 + 2a_0a_1 + a_1^2), \tag{15}$$

$$l_{1,2} = a_0(1 - a_1^2), \tag{16}$$

$$m_{1,0} = 2a_1, \tag{17}$$

$$m_{1,1} = a_0, \tag{18}$$

$$m_{1,2} = a_0, \tag{19}$$

and the coefficients for $j = 2,\ldots,P$ are

$$l_{j,j-1} = a_j(1 - a_{j-1}^2), \tag{20}$$

$$l_{j,j} = a_j(1 + a_{j-1}^2) + a_{j-1}(1 + a_j^2), \tag{21}$$

$$l_{j,j+1} = a_{j-1}(1 - a_j^2), \tag{22}$$

$$m_{j,j-1} = a_j, \tag{23}$$

$$m_{j,j} = a_{j-1} + a_j, \tag{24}$$

$$m_{j,j+1} = a_{j-1}. \tag{25}$$

We note that the ABC Eq. (12) for the auxiliary variables ϕ_j involve wave-like operators on the boundary, and have a symmetric structure.

Initial and edge conditions for the $\phi_j(y,t)$ also have to be specified. From the assumption that the support of the initial solution u is bounded away from the artificial boundary we have

$$\phi_j(y,0) = 0, \quad \partial_t\phi_j(y,0) = 0. \tag{26}$$

The edge conditions can be deduced from (4) and the recursive relations (7) and (8) to be

$$\partial_y\phi_j(0,t) = \partial_y\phi_j(b,t) = 0. \tag{27}$$

We finally note that by considering the first order form (7)–(9) transformed to the frequency domain the connection with PML becomes clear. Solving for the space derivatives we observe that the recursion relations are formally equivalent to a difference approximation with a purely imaginary, frequency-dependent mesh

width, similar to what is suggested in [25]. To produce a discretization of a standard PML one would have to add a real part to the mesh width. Our evanescent mode corrections effectively accomplish this, though in non-standard form.

3. Properties of the basic H–W ABCs

In [19] the reflection coefficient associated with the H–W ABC of order P was calculated using the recursive relations (7)–(9). Here we shall rederive the same result using the ABC (11)–(25) itself. The advantage of this derivation is that it is more direct and will provide us with some additional information. We do, however, recall the results of [21] which emphasize that the actual accuracy of the method depends on more than the magnitude of the reflection coefficients computed here.

We ignore the north and south walls of the guide, namely the boundary conditions (4), and consider a solution u in the form of a propagating plane wave with a given angle of incidence θ. (Alternatively, we may consider "wave guide modes" which take into account the guide wall conditions; the analysis is essentially the same and the results are identical.) Thus, we take

$$u = \exp[\mathrm{i}k(ct - x\cos\theta - y\sin\theta)] + R\exp[\mathrm{i}k(ct + x\cos\theta - y\sin\theta)]. \tag{28}$$

Here i is the imaginary unit, k is the wave number, and θ is the angle of incidence. The first term on the right side represents an outgoing wave, whereas the second term represents a wave spuriously reflected from the artificial boundary, and its coefficient R is the reflection coefficient. We assume a similar form for all the auxiliary variables:

$$\phi_j = \eta_j \exp[\mathrm{i}k(ct - x\cos\theta - y\sin\theta)] + \rho_j \exp[\mathrm{i}k(ct + x\cos\theta - y\sin\theta)]. \tag{29}$$

We substitute these expressions into the equations of the ABC (11)–(25), assuming for simplicity that $a_j = 1$ for all j. This yields a linear system of algebraic equations for the coefficients R, η_j and ρ_j. We note that only the sum $\mu_j = \eta_j + \rho_j$ appears in these equations and not η_j or ρ_j separately. In matrix form, these equations are:

$$\begin{bmatrix} 1+\cos\theta & -1 & 0\cdots & & & \\ -2S & 4-S & -S & 0\cdots & & \\ 0 & -S & 4-2S & -S & 0\cdots & \\ \vdots & & \ddots & & & \\ \cdots & & \cdots 0 & -S & 4-2S & -S \\ \cdots & & & \cdots 0 & -S & 4-2S \end{bmatrix} \begin{Bmatrix} R \\ \mu_1 \\ \mu_2 \\ \vdots \\ \mu_{P-1} \\ \mu_P \end{Bmatrix} = \begin{Bmatrix} -(1-\cos\theta) \\ 2S \\ 0 \\ 0 \\ \vdots \\ 0 \end{Bmatrix}, \tag{30}$$

where $S = \sin^2\theta$.

Now we start to "strip off" this system and express each of the μ_j in terms of R. First, from the first equation of the system (30) we get

$$\mu_1 = (1-\cos\theta) + R(1+\cos\theta). \tag{31}$$

Then, the second equation of (30) yields:

$$S\mu_2 = -2SR + (4-S)\mu_1 - 2S. \tag{32}$$

We substitute the expression for μ_1 given by (31) to obtain

$$S\mu_2 = -2S + (4-S)(1-\cos\theta) + R(-2S + (4-S)(1+\cos\theta)). \tag{33}$$

Simple algebra gives the identities

$$-2S + (4-S)(1\pm\cos\theta) = (1\pm\cos\theta)^3. \tag{34}$$

Thus (32) yields

$$S\mu_2 = (1-\cos\theta)^3 + R(1+\cos\theta)^3. \tag{35}$$

Next, the third equation of (30) gives

$$S\mu_3 = -S\mu_1 + (4-2S)\mu_2. \tag{36}$$

We multiply both sides by S and substitute the expressions above for μ_1 and μ_2, thus obtaining

$$S^2\mu_3 = -S^2(1-\cos\theta) + (4-2S)(1-\cos\theta)^3 + R[-S^2(1+\cos\theta) + (4-2S)(1+\cos\theta)^3]. \tag{37}$$

Simple algebra gives the identities

$$-S^2(1\pm\cos\theta) + (4-2S)(1\pm\cos\theta)^3 = (1\pm\cos\theta)^5. \tag{38}$$

Thus we get

$$S^2\mu_3 = (1-\cos\theta)^5 + R(1+\cos\theta)^5. \tag{39}$$

From now on, the pattern repeats itself, and we obtain similarly

$$S^3\mu_4 = (1-\cos\theta)^7 + R(1+\cos\theta)^7. \tag{40}$$

Proceeding inductively, the one before last equation in (30) gives us finally:

$$(\sin\theta)^{2P-2}\mu_P = (1-\cos\theta)^{2P-1} + R(1+\cos\theta)^{2P-1}. \tag{41}$$

The last equation of (30) gives us the reflection coefficient R. This equation is

$$-S\mu_{P-1} + (4-2S)\mu_P = 0. \tag{42}$$

Substituting the expressions for μ_{P-1} and μ_P from (41) results, after some manipulation, in

$$R = -\left(\frac{1-\cos\theta}{1+\cos\theta}\right)^{2P+1}. \tag{43}$$

This is indeed the reflection coefficient derived in a less direct way in [19]. It can be shown that in the more general case, where the parameters a_j take any chosen values, the reflection coefficient becomes

$$R = \left|\frac{a_0-\cos\theta}{a_0+\cos\theta}\right| \prod_{j=1}^{P}\left(\frac{a_j-\cos\theta}{a_j+\cos\theta}\right)^2. \tag{44}$$

Thus, the reflection coefficient tends to zero exponentially fast as P approaches infinity, regardless of the values of the parameters a_j. Owing to the power two appearing in the expression, the rate of convergence of R is twice as large as that associated with the Givoli–Neta formulation [17] (or with the theoretical Higdon ABC).

In [21] we have proposed and used an adaptive scheme based on the norm of the last auxiliary variable, ϕ_P. Namely, we assumed that $\|\phi_P\|$ is a good indicator for estimating $|R|$, and thus increased the order P when at a certain time step $\|\phi_P\|$ was not sufficiently small. Now we are in a position to check this assumption, by obtaining an explicit expression for μ_P. By using (43) in (41) and manipulating we obtain

$$\mu_P = \frac{4\cos\theta}{1+\cos\theta}\left(\frac{1-\cos\theta}{1+\cos\theta}\right)^P. \tag{45}$$

From (45) and (43) we also obtain the relation

$$|\mu_P| = \left|\frac{4\cos\theta}{1+\cos\theta}\right| |R|^{P/(2P+1)}. \tag{46}$$

Writing this differently we get

$$|R| = (\alpha(\theta;P)\,|\mu_P|)^{2+1/P}, \tag{47}$$

where

$$\alpha(\theta;P) = \frac{1+\cos\theta}{4\cos\theta}. \tag{48}$$

This relation supports the adaptive strategy proposed in [21] in that it establishes a monotone relation between $|\mu_P|$ and $|R|$.

We note, however, that if the incident wave is very oblique ($\cos\theta \ll 1$) then, due to the fact that $\alpha(\theta)$ is not bounded from above the estimate of $|R|$ based on $|\mu_P|$ may be ineffective. An estimate that circumvents this difficulty is one based on the *ratio* between μ_P and μ_{P-1}. Simple calculation gives

$$|R| = \left(\beta(\theta;P)\left|\frac{\mu_P}{\mu_{P-1}}\right|\right)^{2P+1}, \tag{49}$$

where

$$\beta(\theta;P) = \frac{2(1+\cos^2\theta)}{(1+\cos\theta)^2}. \tag{50}$$

Since $1 \leqslant \beta \leqslant 2$, the estimate (49) is expected to be a better choice in an adaptive scheme (at least for P values not very large) than (47).

For completeness, we end this section by quoting additional properties of the H–W ABC, which have already been discussed in [20]:

- *Decay of the auxiliary variables*. For an incident wave field consisting solely of a propagating plane wave, the magnitude of the auxiliary variable ϕ_j becomes smaller as j increases, and approaches zero as $j \to \infty$, regardless of the choice of the parameters a_j.
- *Computational complexity*: The ABC has $O(PN_{\mathcal{B}})$ complexity per time-step, where $N_{\mathcal{B}}$ is the number of nodes on the boundary. In other words, the computational effort associated with the boundary treatment increases *linearly* with the order P of the ABC. This effort is typically marginal (even for quite a large P) with respect to the total effort required by the entire solution process.
- *Accuracy*. Numerical experiments for the exterior problem [20] show that for a fixed simulation time, the solution corresponding to the truncated problem with the ABC imposed, converges exponentially to the exact solution as the order P approaches infinity. This is consistent with the convergence analysis presented (for slightly different cases) in [15,23].
- *Stability*. The H–W formulation for a half-space (i.e. assuming an infinite artificial boundary) is strongly hyperbolic, and hence well-posed. Numerical experiments show (see [20,21]) that finite difference and finite element discretization yield a stable scheme, and that stability is maintained even for very long simulation times.

4. Error generated by truncating the exact operator

The P-order ABC (11)–(13) may be written concisely as

$$(a_0\partial_t + c\partial_x)u + a_0 M_P u = 0, \tag{51}$$

where M_P is a linear operator. This is not merely an abstract notation; for given u on the boundary $\mathcal{B}$ one can actually compute $M_P u$ by using (12) and (13). The latter constitute P equations for the P unknowns $\phi_1, \ldots, \phi_P$. In particular one may solve for ϕ_1, and from it calculate

$$M_P u \equiv -\partial_t \phi_1. \tag{52}$$

We may also consider a theoretical *exact boundary condition* of the form

$$(a_0\partial_t + c\partial_x)u + a_0 M u = 0, \tag{53}$$

where M is the exact boundary operator. Assuming that the ABC converges we must have $M = \lim_{P\to\infty} M_P$ (see below). It is then interesting to examine the error generated by truncating the exact operator, namely to calculate $\|Mu - M_P u\|$ for some representative solution u and an appropriate norm $\|\cdot\|$. We do this numerically in this section. A somewhat similar calculation was done in de Castro's thesis [29].

We again consider a propagating plane wave solution. (We may alternatively consider "wave guide modes," leading to the same results.) In contrast to (28) and (29), we ignore reflected waves and assume functions of the form

$$u = \exp[\mathrm{i}k(ct - x\cos\theta - y\sin\theta)], \tag{54}$$

$$\phi_j = \eta_j \exp[\mathrm{i}k(ct - x\cos\theta - y\sin\theta)], \tag{55}$$

which are plane waves with angle of incidence θ. We substitute these into the P-order ABC Eqs. (12) and (13), taking $a_j = 1$ as before for simplicity. This gives us a system of equations for the coefficients η_j, which we denote $\eta_j^{(P)}$ to emphasize that they are obtained by a P-order ABC. In matrix form this system is

$$\begin{bmatrix} 4-S & -S & 0\ldots & & \\ -S & 4-2S & -S & 0\ldots & \\ 0 & -S & 4-2S & -S\ldots & \\ \vdots & & & \ddots & \\ & \ldots 0 & -S & 4-2S & -S \\ & & \ldots 0 & -S & 4-2S \end{bmatrix} \begin{Bmatrix} \eta_1^{(P)} \\ \eta_2^{(P)} \\ \vdots \\ \vdots \\ \eta_{P-1}^{(P)} \\ \eta_P^{(P)} \end{Bmatrix} = \begin{Bmatrix} 2S \\ 0 \\ \vdots \\ \vdots \\ 0 \\ 0 \end{Bmatrix}, \tag{56}$$

where $S = \sin^2\theta$. Note that this system can be obtained from (30) by truncating the first row and column in the latter.

Since the ABC for u is determined by ϕ_1 (see (51) and (52)), the goal in solving (56) is to find $\eta_1^{(P)}$. Once $\eta_1^{(P)}$ is found, we may calculate

$$M_P u = -\partial_t \phi_1^{(P)} = \mathrm{i}kc\eta_1^{(P)} \exp[\mathrm{i}k(ct - x\cos\theta - y\sin\theta)]. \tag{57}$$

This should be compared with the exact value

$$Mu = -\partial_t \phi_1 = \mathrm{i}kc\eta_1 \exp[\mathrm{i}k(ct - x\cos\theta - y\sin\theta)]. \tag{58}$$

Here η_1 may be calculated by substituting (54) and (55) in (11), which gives $\eta_1 = 1 - \cos\theta$. Thus the error generated by the P-order operator may be measured via

$$E^{(P)} = \left|1 - \frac{\eta_1^{(P)}}{\eta_1}\right| = \left|1 - \frac{\eta_1^{(P)}}{1-\cos\theta}\right|. \tag{59}$$

It is possible to prove that indeed

$$\lim_{P\to\infty} \eta_1^{(P)} = \eta_1 = 1 - \cos\theta, \tag{60}$$

and thus the operator truncation error approaches zero as P tends to infinity. The proof is given in Appendix A.

Fig. 2 shows the variation of the error $E^{(P)}$ as a function of the order P for various values of the incident angle θ. $P = 0$ corresponds to the Sommerfeld-like boundary condition $(\partial_t + c\partial_x)u = 0$. The convergence with increasing P is clearly exponential, and the convergence slope (which is the power β in the expression $E^{(P)} = C\exp(-\beta P)$) decreases with increasing angle of incidence θ. For angles of incidence nearly normal to the boundary the convergence is extremely fast; this is due to our choice of parameters $a_j = 1$. However, even for very oblique incidence ($\theta = 85^\circ$) the ABC truncation error becomes very small for practical values of P (e.g. $E = 10^{-10}$ for $P = 60$). This demonstrates the robustness of the ABC and the fact that one may generally be content with the simple choice $a_j = 1$.

It is expected that the behavior of the ABC truncation error be similar to that of the reflection coefficient R. We therefore compare the convergence slopes obtained in Fig. 2 for $E^{(P)}$ with those predicted by the expression (43) for R. This comparison is shown in Fig. 3 where the two error measures are plotted as a function of the

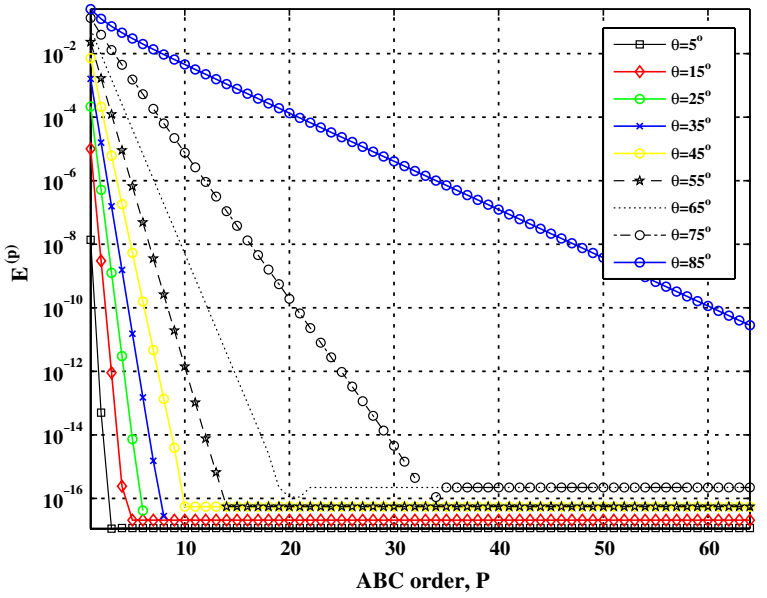

Fig. 2. ABC operator truncation error as a function of the order P, for various values of the incident angle θ.

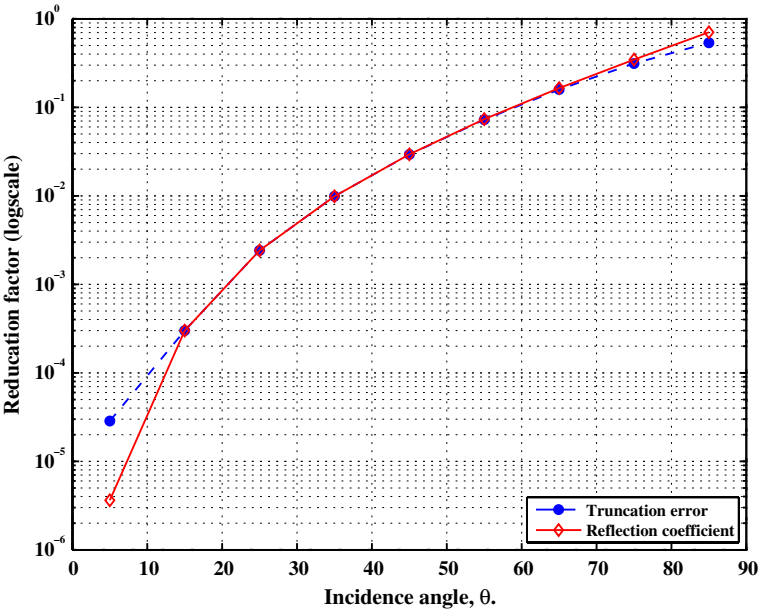

Fig. 3. Comparison between the convergence slopes associated with the ABC operator truncation error (Fig. 2) and with the reflection coefficient R (as predicted by (43)), as a function of the angle of incidence θ.

angle of incidence. We see that indeed they behave very similarly, except at nearly normal incidence. The discrepancy in the latter case may partly be attributed to error in measuring the very steep slope for $\theta = 5^\circ$ in Fig. 2.

We do, however, remind the reader that the representation of the solution in terms of propagating plane waves is incomplete. Particularly for long time (low frequency) simulations significantly more accurate results can be obtained if the evanescent modes are explicitly treated.

5. Dispersive medium

We now consider the case of a dispersive medium, such as the atmosphere or ocean when earth rotation is taken into account (see, e.g. Pedlosky [30]). This amounts to including a non-differentiated term in the wave equation, which then becomes the Klein–Gordon equation. Thus (1) and (6) are replaced, respectively, by

$$\partial_t^2 u - c^2\nabla^2 u + f^2 u = s \quad \text{in } \Omega, \tag{61}$$

$$\partial_t^2 u - c^2\nabla^2 u + f^2 u = 0 \quad \text{in } D. \tag{62}$$

We assume that in D (and on Γ_E) f is constant. In Ω, f may be a function of location.

We define the auxiliary variables ϕ_j by using the same recursive relations (7)–(9) as in the non-dispersive case. Then working along the same line as in Section 2, we easily arrive at the conclusion that the ABC Eq. (12) remains unchanged except that all occurrences of $c^2\partial_y^2$ should be replaced by $c^2\partial_y^2 - f^2$. Thus the ABC of order P is

$$(a_0\partial_t + c\partial_x)u = a_0\partial_t\phi_1, \tag{63}$$

$$\begin{aligned} &l_{j,j-1}\partial_t^2\phi_{j-1} + l_{j,j}\partial_t^2\phi_j + l_{j,j+1}\partial_t^2\phi_{j+1} \\ &\quad = c^2\left(m_{j,j-1}\partial_y^2\phi_{j-1} + m_{j,j}\partial_y^2\phi_j + m_{j,j+1}\partial_y^2\phi_{j+1}\right) \\ &\qquad - f^2\left(m_{j,j-1}\phi_{j-1} + m_{j,j}\phi_j + m_{j,j+1}\phi_{j+1}\right), \quad j = 1,\ldots,P, \end{aligned} \tag{64}$$

$$\phi_0 \equiv u, \quad \phi_{P+1} = 0, \tag{65}$$

with the same coefficients as given by (14)–(25).

6. Stratified medium

6.1. Preliminary remark

If the medium is inhomogeneous, namely $c = c(\boldsymbol{x})$, there are a number of versions for the wave equation, depending on the physical context. Two versions that we shall consider are

$$\nabla^2 u = \frac{1}{c^2(\boldsymbol{x})}\partial_t^2 u, \tag{66}$$

and

$$\nabla\cdot(c^2(\boldsymbol{x})\nabla u) = \partial_t^2 u. \tag{67}$$

For example, Eq. (67) is obtained from the linearized shallow water equations in the case of a flat bottom, where u is the water surface height (see Pedlosky [30]). In acoustics, if one assumes that the wave speed changes as a function of location much more significantly than the density, one is led to an equation of the form (66) for the pressure (see [31]).

We shall extend the ABC in the case of a stratified medium for each of these two wave equations.

6.2. Layers

6.2.1. Interface conditions

If $c = c(\boldsymbol{x})$ is piecewise-constant then we are talking about the case of *layers*. In this case the wave equation with a constant wave speed holds inside each layer. On the interfaces between the layers, continuity conditions are necessary to define a unique solution. One condition is the continuity of u itself; a second condition involves the continuity of a quantity related to the normal derivative of u. Such conditions can easily be

obtained in a variational manner. For example, consider Eq. (66). Its weak form, assuming for simplicity zero Dirichlet or Neumann boundary conditions, is

$$\int_\Omega w\frac{1}{c^2}\partial_t^2 u\,\mathrm{d}\Omega+\int_\Omega \nabla w\cdot\nabla u\,\mathrm{d}\Omega=0$$

for an arbitrary w belonging to the weighting space. We write each integral as a sum of integrals over the layers (or over the elements in a finite element context):

$$\sum_e\int_{\Omega^e} w\frac{1}{c^2}\partial_t^2 u\,\mathrm{d}\Omega+\sum_e\int_{\Omega^e}\nabla w\cdot\nabla u\,\mathrm{d}\Omega=0.$$

We use the divergence theorem to manipulate the second term and get

$$\sum_e\int_{\Omega^e} w\frac{1}{c^2}\partial_t^2 u\,\mathrm{d}\Omega+\sum_e\left(\int_{\partial\Omega^e} w\frac{\partial u}{\partial n}\,\mathrm{d}\Gamma-\int_{\Omega^e} w\nabla^2 u\,\mathrm{d}\Omega\right)=0.$$

Since the wave equation holds in each layer (element), we get

$$\sum_e\int_{\partial\Omega^e} w\frac{\partial u}{\partial n}\,\mathrm{d}\Gamma=0.$$

From the arbitrariness of w, and concentrating on a single interface $\partial\Omega_{12}$ between two layers, we have

$$\int_{\partial\Omega_{12}} w\left(\frac{\partial u}{\partial n_1}+\frac{\partial u}{\partial n_2}\right)\mathrm{d}\Gamma=0.$$

Since $\boldsymbol{n}_1=-\boldsymbol{n}_2$, this gives

$$\int_{\partial\Omega_{12}} w\left[\frac{\partial u}{\partial n}\right]\mathrm{d}\Gamma=0,$$

where $[\cdot]$ denotes the *jump* across the interface. From this weak condition we conclude the strong condition $\left[\frac{\partial u}{\partial n}\right]=0$. Thus, the two continuity conditions corresponding to the wave Eq. (66) are:

$$[u]=0,\quad \left[\frac{\partial u}{\partial n}\right]=0. \tag{68}$$

Here $\partial/\partial n$ is the normal derivative on the interface between the layers. In the context of a wave guide with horizontal layers, $\partial/\partial n=\partial/\partial y$.

In a similar manner we obtain the continuity conditions corresponding to the wave Eq. (67). They are:

$$[u]=0,\quad \left[c^2\frac{\partial u}{\partial n}\right]=0. \tag{69}$$

6.2.2. ABC for layered media

We assume that the wave guide consists of horizontal layers, each with its own wave speed. We consider the wave Eq. (67), with continuity conditions (69). The corresponding ABC in each layer has the form (11)–(13). Let us obtain continuity conditions for the auxiliary variables ϕ_j. We will require all the ϕ_j to be continuous across the interfaces. It remains to find the second continuity condition for the ϕ_j.

We start with the ABC Eq. (11) for u. Writing it for each layer k separately we have

$$(a_0^{(k)}\partial_t+c^{(k)}\partial_x)u^{(k)}=a_0^{(k)}\partial_t\phi_1^{(k)}. \tag{70}$$

Here (k) indicates layer k. Dividing by $a_0^{(k)}$ we have

$$\left(\partial_t + \frac{c^{(k)}}{a_0^{(k)}}\partial_x\right) u^{(k)} = \partial_t \phi_1^{(k)}. \tag{71}$$

All the quantities in this equation except the coefficient c/a_0 are continuous. Therefore we must require that c/a_0 be continuous too. This leads to the choice $a_0^{(k)} = A_0 c^{(k)}$, where A_0 is a constant which does not depend on the layer.

Now we differentiate the ABC (71) with respect to y, and then multiply by c^2, to obtain

$$\left(\partial_t + \frac{c^{(k)}}{a_0^{(k)}}\partial_x\right)\left((c^2)^{(k)}\partial_y u^{(k)}\right) = (c^2)^{(k)}\partial_{ty}\phi_1^{(k)}. \tag{72}$$

The left side of this equation is continuous. Hence the right side must also be continuous. This means that $p_y\phi_1^{(k)}$ is continuous. We thus obtain the following conditions for ϕ_1:

$$[\phi_1] = 0, \quad \left[c^2\partial_y\phi_1\right] = 0, \tag{73}$$

which are identical to the conditions (69) for u.

In a similar fashion, and proceeding by induction, we can show that one should take

$$a_j^l = \frac{c_l}{c_0}\bar{a}_j. \tag{74}$$

Here $\bar{a}_j$ are layer-independent parameters which should be chosen *a priori*; they have the same role as the a_j in the homogeneous case. We see that even if we make the simplest choice $\bar{a}_j = 1$ for all j, the parameters a_j^l which appear in the ABC will vary from layer to layer. The c_0 in (74) is a reference wave speed; for example,

$$c_0 = \max_l c_l. \tag{75}$$

Using the a_j^l given by (74) in (11)–(25) implies that all the coefficients l and m in (12) also become layer-dependent. With the choice of parameters (74), the jump conditions for the ϕ_j are similar to those for u, namely

$$[\phi_j] = 0, \quad [c^2\partial_y\phi_j] = 0. \tag{76}$$

We now consider the wave Eq. (66), with continuity conditions (68). The corresponding ABC is again (11)–(13). Following the same lines of derivation as above, we conclude that the choice (74) should be made here too, which leads to the continuity conditions

$$[\phi_j] = 0, \quad \left[\partial_y\phi_j\right] = 0 \tag{77}$$

for all the ϕ_j.

We note that in the finite difference method one has to discretize the conditions (76) or (77) directly and append them to the interior discrete equations. In contrast, in the finite element method these jump conditions are enforced weakly by the variational formulation as natural boundary conditions [32]. Thus, with finite element discretization in space, no direct enforcement of these conditions is necessary.

6.3. Continuous wave speed variation

Now we assume that the wave speed varies in the cross-section of the wave guide continuously, i.e. $c = c(y)$.

A crucial step in passing from the recursive relations (7)–(9) to the ABC is the use of the fact that each ϕ_j satisfies the wave equation (see (10)). This cannot be shown if $c = c(y)$ and (7)–(9) are taken with constant parameters a_j. One needs to consider variable a_j, namely $a_j = a_j(y)$. Analogously to the case of layers, we define (cf. (74))

$$a_j(y) = \frac{c(y)}{c_0}\bar{a}_j, \tag{78}$$

where the $\bar{a}_j$ are chosen constant parameters (e.g. $\bar{a}_j = 1$ for all j) and c_0 is a reference wave speed, say $c_0 = \max_{y\in[0,b]} c(y)$. With this choice the y-dependence cancels out from the recursive relations (7)–(9) and they become

$$(\bar{a}_0\partial_t + c_0\partial_x)u = \bar{a}_0\partial_t\phi_1, \tag{79}$$

$$(\bar{a}_j\partial_t + c_0\partial_x)\phi_j = (\bar{a}_j\partial_t - c_0\partial_x)\phi_{j+1}, \quad j = 1,\ldots,P, \tag{80}$$

$$\phi_{P+1} = 0. \tag{81}$$

Using these constant-coefficient recursive relations it is easy to show, by induction, that each ϕ_j satisfies the wave equation. It is also possible to obtain an expression for the reflection coefficient R analogous to that obtained in the homogeneous case, (44) (with $\bar{a}_j$ replacing a_j), except that one cannot interpret the results directly in terms of an incidence angle. One must, of course, replace the plane wave solutions with appropriate modal solutions of the variable coefficient problem.

It now remains to derive the ABC from the recursive relations. This is done using the same manipulations as in the homogeneous case. With the wave Eq. (66) and $c = c(y)$, the ABC equations remain exactly as in (11)–(13), but with the constant c and a_j replaced by $c(y)$ and $a_j(y)$ everywhere. On the other hand, with the wave Eq. (67), the ABC Eq. (12) must be rewritten in the form

$$l_{j,j-1}\partial_t^2\phi_{j-1} + l_{j,j}\partial_t^2\phi_j + l_{j,j+1}\partial_t^2\phi_{j+1} = m_{j,j-1}\partial_y(c^2\partial_y\phi_{j-1}) + m_{j,j}\partial_y(c^2\partial_y\phi_j) + m_{j,j+1}\partial_y(c^2\partial_y\phi_{j+1}),$$
$$j = 1,\ldots,P. \tag{82}$$

All the other expressions remain unchanged. In all cases, it is important to use the y-dependent parameters a_j defined by (78) in the expressions for $l_{j,i}$ and $m_{j,i}$ given in (14)–(25).

7. Inclusion of evanescent modes

7.1. Derivation

In general, a solution to the wave Eq. (1) can be written as a superposition of propagating and evanescent plane waves. The ABC (11)–(13) takes into account only propagating modes. Ignoring the evanescent modes may be justified in many cases, since they decay exponentially away from their origin. However, in some situations the evanescent mode content in the solution may be significant, e.g. when the artificial boundary is very close to a source or to a physical boundary. In particular, if one requires very high accuracy, the evanescent modes must not be ignored. In fact, without taking account of these modes, our arguments do not imply that the ABC converges as $P \to \infty$. (More elaborate analysis does, in fact, show that there is convergence for finite times. See e.g. [15].)

In the present context, for an artificial boundary whose normal direction is x, an evanescent mode has the form $\exp(-\sigma x)V(y,t;\sigma)$. The decay rate σ characterizes the evanescent mode just as the cosine of angle of incidence $a = \cos\theta$ characterizes the propagating mode. More precisely, the solution at a point on the boundary may be represented by the formula

$$u(x,t) = \int_0^{\pi/2} G(ct - x\cos\theta, y)\,\mathrm{d}\theta + \int_0^{\infty} \mathrm{e}^{-\sigma x} V(y,t;\sigma)\,\mathrm{d}\sigma. \tag{83}$$

Here the first integral represents the propagating modes and the second integral represents the evanescent modes. This formula, which is inspired by the plane wave translation formula from the Helmholtz fast multipole method [33], is straightforward to derive from a Fourier–Laplace representation of the solution in $x > -\delta$ using data at $x = -\delta$, where δ is the distance (in the x direction) between the boundary and the location of the source (nonzero s in (1) or u_0, v_0 in (5)) closest to it.

Given this representation, local boundary conditions with $P + E$ auxiliary functions can now be constructed independent of the functions G and V. A more general discussion of this approach is given in [27], where they are termed complete radiation conditions. Precisely, we replace the recursion (7)–(9) by

$$a_0\partial_t u + c\partial_x u = a_0\partial_t \phi_1, \tag{84}$$

$$a_j\partial_t \phi_j + c\partial_x \phi_j = a_j\partial_t \phi_{j+1} - c\partial_t \phi_{j+1}, \quad j = 1,\dots,P, \tag{85}$$

$$\sigma_j \phi_{P+j} + \partial_x \phi_{P+j} = \sigma_j \phi_{P+j+1} - \partial_x \phi_{P+j+1}, \quad j = 1,\dots,E, \tag{86}$$

$$\phi_0 \equiv u, \quad \phi_{P+E+1} = 0. \tag{87}$$

Here the a_j and σ_j are parameters that have to be chosen. See discussion at the end of this section.

We now derive equations along the boundary satisfied by the auxiliary functions, ϕ_j. As in the case of the pure propagation ABC, it is easy to prove inductively that all ϕ_j satisfy the homogeneous scalar wave equation in a neighborhood of the boundary. We begin by manipulating (85) for $1 < j < P$, using the wave equation to eliminate x-derivatives. This yields the ABC Eq. (12). In a similar fashion we manipulate (86) for $j = 2,\dots,E$ to obtain:

$$\begin{aligned}\bar{l}_{j,j-1}\partial_t^2 \phi_{P+j-1} + \bar{l}_{j,j}\partial_t^2 \phi_{P+j} + \bar{l}_{j,j+1}\partial_t^2 \phi_{P+j+1} &= c^2\left(\bar{m}_{j,j-1}\partial_y^2 \phi_{P+j-1} + \bar{m}_{j,j}\partial_y^2 \phi_{P+j} + \bar{m}_{j,j+1}\partial_y^2 \phi_{P+j+1}\right)\\ &\quad + c^2\left(\bar{s}_{j,j-1}\phi_{P+j-1} + \bar{s}_{j,j}\phi_{P+j} + \bar{s}_{j,j+1}\phi_{P+j+1}\right).\end{aligned} \tag{88}$$

The coefficients $\bar{l}_{i,j}$, $\bar{m}_{i,j}$ and $\bar{s}_{i,j}$ will be defined below. Two additional equations are required at the "seam" between the propagating-mode conditions and the evanescent-mode conditions. These equations are formed from (85) for $j = P$ and (86) for $j = 1$. Directly we have:

$$\frac{1 + a_P^2}{a_P}\partial_t^2 \phi_{P+1} + \frac{1 - a_P^2}{a_P} - \frac{c^2}{a_P}\left(\partial_y^2 \phi_{P+1} + \partial_y^2 \phi_P\right) = 2c\partial_{xt}\phi_{P+1}, \tag{89}$$

$$\frac{1}{\sigma_1}\left(\partial_t^2 \phi_{P+1} + \partial_t^2 \phi_{P+2}\right) - \frac{c^2}{\sigma_1}\left(\partial_y^2 \phi_{P+1} + \partial_y^2 \phi_{P+2}\right) + c^2\sigma_1\left(\phi_{P+1} - \phi_{P+2}\right) = -2c^2\partial_x \phi_{P+1}. \tag{90}$$

There are a variety of ways to combine these equations and eliminate the x-derivative. We choose what seems to be the simplest. We define an additional auxiliary function – the seam function ψ – by the relation

$$a_P\partial_t^2 \psi = -2c\partial_{xt}\phi_{P+1}. \tag{91}$$

Then we have:

$$l_{P+1,P}\partial_t^2 \phi_P + l_{P+1,\psi}\partial_t^2 \psi + l_{P+1,P+1}\partial_t^2 \phi_{P+1} = c^2\left(m_{P+1,P}\partial_y^2 \phi_P + m_{P+1,P+1}\partial_y^2 \phi_{P+1}\right), \tag{92}$$

$$\bar{l}_{1,1}\partial_t^2 \phi_{P+1} + \bar{l}_{1,2}\partial_t^2 \phi_{P+2} - c\partial_t \psi = c^2\left(\bar{m}_{1,1}\partial_y^2 \phi_{P+1} + \bar{m}_{1,2}\partial_y^2 \phi_{P+2}\right) + c^2\left(\bar{s}_{1,1}\phi_{P+1} + \bar{s}_{1,2}\phi_{P+2}\right). \tag{93}$$

The coefficients in these equations are defined below.

The (P,E)-order ABC consists of (84), (12) (for $j = 1,\dots,P$), (92) and (93) (the two seam equations), (88) (for $j = 2,\dots,E$) and (87). For clarity, we give here the complete ABC together with the definition of all the coefficients:

$$a_0\partial_t u + c\partial_x u = a_0\partial_t \phi_1, \tag{94}$$

$$l_{j,j-1}\partial_t^2 \phi_{j-1} + l_{j,j}\partial_t^2 \phi_j + l_{j,j+1}\partial_t^2 \phi_{j+1} = c^2\left(m_{j,j-1}\partial_y^2 \phi_{j-1} + m_{j,j}\partial_y^2 \phi_j + m_{j,j+1}\partial_y^2 \phi_{j+1}\right), \quad j = 1,\dots,P, \tag{95}$$

$$l_{P+1,P}\partial_t^2 \phi_P + l_{P+1,\psi}\partial_t^2 \psi + l_{P+1,P+1}\partial_t^2 \phi_{P+1} = c^2\left(m_{P+1,P}\partial_y^2 \phi_P + m_{P+1,P+1}\partial_y^2 \phi_{P+1}\right), \tag{96}$$

$$\bar{l}_{1,1}\partial_t^2 \phi_{P+1} + \bar{l}_{1,2}\partial_t^2 \phi_{P+2} - c\partial_t \psi = c^2\left(\bar{m}_{1,1}\partial_y^2 \phi_{P+1} + \bar{m}_{1,2}\partial_y^2 \phi_{P+2}\right) + c^2(\bar{s}_{1,1}\phi_{P+1} + \bar{s}_{1,2}\phi_{P+2}), \tag{97}$$

$$\begin{aligned}\bar{l}_{j,j-1}\partial_t^2 \phi_{P+j-1} + \bar{l}_{j,j}\partial_t^2 \phi_{P+j} + \bar{l}_{j,j+1}\partial_t^2 \phi_{P+j+1} &= c^2\left(\bar{m}_{j,j-1}\partial_y^2 \phi_{P+j-1} + \bar{m}_{j,j}\partial_y^2 \phi_{P+j} + \bar{m}_{j,j+1}\partial_y^2 \phi_{P+j+1}\right)\\ &\quad + c^2\left(\bar{s}_{j,j-1}\phi_{P+j-1} + \bar{s}_{j,j}\phi_{P+j} + \bar{s}_{j,j+1}\phi_{P+j+1}\right), \quad j = 2,\dots,E,\end{aligned} \tag{98}$$

$$\phi_0 \equiv u, \quad \phi_{P+E+1} = 0, \tag{99}$$

where

$$l_{1,0} = 2a_1(1-a_0^2), \quad l_{1,1} = a_0(1+2a_0a_1+a_1^2), \quad l_{1,2} = a_0(1-a_1^2), \tag{100}$$

$$m_{1,0} = 2a_1, \quad m_{1,1} = a_0, \quad m_{1,2} = a_0, \tag{101}$$

For $j = 2, \ldots, P$:

$$l_{j,j-1} = a_j(1-a_{j-1}^2), \quad l_{j,j} = a_j(1+a_{j-1}^2) + a_{j-1}(1+a_j^2), \quad l_{j,j+1} = a_{j-1}(1-a_j^2), \tag{102}$$

$$m_{j,j-1} = a_j, \quad m_{j,j} = a_{j-1} + a_j, \quad m_{j,j+1} = a_{j-1}, \tag{103}$$

Seam coefficients :

$$l_{P+1,P} = \frac{1-a_P^2}{a_P}, \quad l_{P+1,\psi} = a_P, \quad l_{P+1,P+1} = \frac{1+a_P^2}{a_P}, \tag{104}$$

$$m_{P+1,P} = m_{P+1,P+1} = \frac{1}{a_P}, \tag{105}$$

$$\bar{l}_{1,1} = \bar{m}_{1,1} = \bar{l}_{1,2} = \bar{m}_{1,2} = \frac{1}{\sigma_1 a_P}, \quad \bar{s}_{1,1} = -\frac{\sigma_1}{a_P}, \quad \bar{s}_{1,2} = \frac{\sigma_1}{a_P}, \tag{106}$$

For $j = 2, \ldots, E$:

$$\bar{l}_{j,j-1} = \bar{m}_{j,j-1} = \frac{1}{\sigma_{j-1}}, \quad \bar{l}_{j,j} = \bar{m}_{j,j} = \frac{1}{\sigma_j} + \frac{1}{\sigma_{j-1}}, \quad \bar{l}_{j,j+1} = \bar{m}_{j,j+1} = \frac{1}{\sigma_j}, \tag{107}$$

$$\bar{s}_{j,j-1} = \sigma_{j-1}, \quad \bar{s}_{j,j} = -(\sigma_{j-1} + \sigma_j), \quad \bar{s}_{j,j+1} = \sigma_j. \tag{108}$$

It remains to choose the parameters $0 < a_j \leqslant 1$ and $\sigma_j > 0$. As mentioned previously the solution is not very sensitive to the values of the a_j, and the choice $a_j = 1$ for all j is a reasonable one. We will also employ parameters which follow from an approximation to the first integral in (83) via the Radau quadrature rule. Precisely $a_j = \cos\theta_j$ with

$$\theta_j = \frac{\pi(c_j+1)}{4}, \quad j = 0, \ldots, P, \tag{109}$$

where the c_j are the left endpoint Gauss–Radau nodes on $[-1, 1]$.

The choice for σ_j is less obvious, mainly because it is not bounded from above, although the analysis of Section 7.2 below suggests that the solution should not be very sensitive to it either. One possible scheme for choosing the σ_j is based on the approximation of the second integral in (83), which represents the evanescent modes, by a quadrature rule:

$$\int_0^\infty \mathrm{e}^{-\sigma x} V(y,t;\sigma)\,\mathrm{d}\sigma \simeq \sum_{j=1}^{E} \mathrm{e}^{-\sigma_j x} V_j(y,t). \tag{110}$$

(Here we include the quadrature weights in the definition of the V_j.) Thus it seems reasonable to choose the σ_j as the quadrature points used in the approximation (110). In our numerical experiments we have chosen σ_j to be the Yarvin–Rokhlin nodes determined by δ, the distance between the boundary and the closest source [34]. We note that the evanescent mode recursion as we have written it is independent of the wave speed. Thus in subsequent applications to layered media the parameter choices for different layers will be identical.

7.2. Reflection coefficient

The fact that the basic ABC (11)–(13) yields a "small" and convergent reflection coefficient (given by (44)) when it encounters a propagating plane wave has been established in Section 3. Since the extended ABC (94)–(99) involves a combination of propagating and evanescent operators it is less clear *a priori* how it would behave in the presence of either propagating or evanescent waves. Now we calculate the reflection coefficients generated by the ABC (94)–(99) in two cases: (1) when a propagating plane wave impinges on the boundary; (2) when a pure evanescent plane wave impinges on the boundary.

We first look for a solution with a right-going propagating wave and a reflected left-going wave:

$$\phi_j = A_j e^{i(k_1 x + k_2 y - \omega t)} + B_j e^{i(-k_1 x + k_2 y - \omega t)}, \tag{111}$$

where $A_0 = 1$ and B_0 is the reflection coefficient. By substituting this form into the recursive relations (84),(87) and proceeding along the same lines as in the case of the basic ABC, we finally obtain

$$B_0 = -\frac{(\omega a_0 - c k_1)}{(\omega a_0 + c k_1)} \prod_{j=1}^{P} \left(\frac{\omega a_j - c k_1}{\omega a_j + c k_1} \right)^2 \cdot \prod_{j=1}^{E} \left(\frac{\sigma_j + i c k_1}{\sigma_j - i c k_1} \right)^2. \tag{112}$$

Clearly, the reflection coefficient is zero if $\omega a_j = c k_1$ for some j. Also, B_0 goes to zero as P tends to infinity. The product over the evanescent factors is a complex number with absolute value of one, and hence does not worsen the convergence.

Now we repeat the calculation assuming a solution consisting of an evanescent mode:

$$\phi_j = A_j e^{-\sigma x + i(k_2 y - \omega t)} + B_j e^{\sigma x + i(k_2 y - \omega t)}, \tag{113}$$

where $A_0 = 1$ and B_0 is the reflection coefficient. In this case we obtain, using the same technique,

$$B_0 = -\frac{(i\omega a_0 + c\sigma)}{(i\omega a_0 - c\sigma)} \prod_{j=1}^{P} \left(\frac{i\omega a_j + c\sigma}{i\omega a_j - c\sigma} \right)^2 \cdot \prod_{j=1}^{E} \left(\frac{\sigma_j - \sigma}{\sigma_j + \sigma} \right)^2. \tag{114}$$

The reflection coefficient is zero if $\sigma_j = \sigma$ for some j. Also, B_0 goes to zero as E tends to infinity. The product over the propagation factors is a complex number with absolute value of one, and hence does not worsen the convergence.

In general, convergence requires *both* $P \to \infty$ and $E \to \infty$. Precise error estimates are given in [27,28].

8. Numerical schemes

8.1. Finite element scheme

We shall describe the Finite Element (FE) formulation for the problem using the *basic* ABC (11)–(13). The extended ABCs discussed in Sections 5–7 require some modifications, which are rather straightforward and for the sake of brevity will not be given here.

We consider the problem consisting of (1) in Ω, the boundary and initial conditions (3)–(5) and the ABC (11)–(13) on Γ_E. The weak form of this problem is:

Find $u \in \mathcal{S}$ and $\phi_j \in H^1(\Gamma_E)$ such that for all $w \in \mathcal{S}$ and all $\psi_j \in H^1(\Gamma_E)$ there holds

$$\int_{\Omega^e} w \partial_t^2 u \, d\Omega + a_0 c \int_{\Gamma_E} w \partial_t u \, d\Gamma + c^2 \int_{\Omega^e} \nabla w \cdot \nabla u \, d\Omega = \int_{\Omega} w s \, d\Omega + a_0 c \int_{\Gamma_E} w \partial_t \phi_1 \, d\Gamma, \tag{115}$$

For $j = 1, \ldots, P$:

$$\begin{aligned} & l_{j,j-1} \int_{\Gamma_E} \psi_j \partial_t^2 \phi_{j-1} \, d\Gamma + l_{jj} \int_{\Gamma_E} \psi_j \partial_t^2 \phi_j \, d\Gamma + l_{j,j+1} \int_{\Gamma_E} \psi_j \partial_t^2 \phi_{j+1} \, d\Gamma \\ & + c^2 \left(m_{j,j-1} \int_{\Gamma_E} \partial_y \psi_j \partial_y \phi_{j-1} \, d\Gamma + m_{j,j} \int_{\Gamma_E} \partial_y \psi_j \partial_y \phi_j \, d\Gamma + m_{j,j+1} \int_{\Gamma_E} \partial_y \psi_j \partial_y \phi_{j+1} \, d\Gamma \right) \\ & = 0. \end{aligned} \tag{116}$$

The space $\mathcal{S}$ is defined by

$$\mathcal{S} = \{ w \mid w \in H^1(\Omega) \quad \text{and} \quad w = 0 \quad \text{on } \Gamma_W \}, \tag{117}$$

H^1 being the Sobolev space of functions in L_2 with first derivatives in L_2. In these equations one should take $\phi_0 = u$ on Γ_E and $\phi_{P+1} = 0$, according to (13).

The standard spatial Galerkin FE discretization of (115) and (116) is employed. On the global level, the variables u and ϕ_j are replaced by their finite-dimensional approximations

$$u^h(\boldsymbol{x},t)=\sum_{A=1}^{N_{h,\Omega}} d_A^h(t)N_A(\boldsymbol{x}),\quad \mathbf{x}\in\Omega,\qquad \phi_j^h(\boldsymbol{s},t)=\sum_{A=1}^{N_{h,\Gamma_{\mathrm{E}}}}\phi_{jA}^h(t)N_A^{(j)}(\boldsymbol{s}),\quad \boldsymbol{s}\in\Gamma_{\mathrm{E}}. \tag{118}$$

Here h is the mesh parameter, A stands for a global node number, N_A is the global-level shape function associated with the variable u^h and node A, and $N_A^{(j)}$ is the global-level shape function associated with variable ϕ_j^h and node A. Note that while N_A is a function defined in two dimensions (say $N_A(x,y)$), the function $N_A^{(j)}$ is one-dimensional (say $N_A^{(j)}(y)$). The expansion analogous to this on the element level is

$$u^e(\boldsymbol{x},t)=\sum_{a=1}^{N_{\mathrm{en}}} d_a^e(t)N_a(\boldsymbol{x}),\quad \mathbf{x}\in\Omega^e,\qquad \phi_j^e(\boldsymbol{s},t)=\sum_{a=1}^{N_{\mathrm{en}}}\phi_{ja}^e(t)N_a^{(j)}(\boldsymbol{s}),\quad \boldsymbol{s}\in\Gamma_{\mathrm{E}}^e. \tag{119}$$

Here Ω^e is the domain of element e, $\Gamma_{\mathrm{E}}^e=\Gamma_{\mathrm{E}}\cap\partial\Omega^e$, N_a is the element shape function associated with u^h and element node a, $N_a^{(j)}$ is the element shape function associated with ϕ_j^h and element node a, d_a^e is the nodal value of u^e at node a of element e, ϕ_{ja}^e is the nodal value of ϕ_j^e at node a of element e, and N_{en} is the number of element nodes. Similar expansions are used for the weight functions w and ψ_j.

The FE formulation allows, at least in theory, a general choice of the shape functions, namely different shape functions $N_a^{(j)}$ may be chosen for the different variables ϕ_j, for $j=0,1,\ldots,P$. We use bilinear or linear shape functions for all the variables, which is a most convenient choice and turns out to be stable. See [20] for discussion on the computational aspects of this choice. In the sequel we shall continue to indicate the variable number j for generality.

Using the approximations (118) in the weak Eqs. (115) and (116) leads to the following system of linear ordinary differential equations (ODEs) in time:

$$\boldsymbol{M}\ddot{\boldsymbol{d}}+\boldsymbol{C}\dot{\boldsymbol{d}}+\boldsymbol{K}\boldsymbol{d}=\boldsymbol{F}+\boldsymbol{G}\dot{\boldsymbol{\phi}}_1, \tag{120}$$

For $j=1,\ldots,P$:

$$\boldsymbol{A}_j\ddot{\boldsymbol{\phi}}_{j-1}+\boldsymbol{B}_j\ddot{\boldsymbol{\phi}}_j+\boldsymbol{D}_j\ddot{\boldsymbol{\phi}}_{j+1}+\boldsymbol{E}_j\boldsymbol{\phi}_{j-1}+\boldsymbol{H}_j\boldsymbol{\phi}_j+\boldsymbol{I}_j\boldsymbol{\phi}_{j+1}=0, \tag{121}$$

$$\boldsymbol{\phi}_0\equiv\boldsymbol{d}|_{\Gamma_{\mathrm{E}}},\qquad \boldsymbol{\phi}_{P+1}=\mathbf{0}. \tag{122}$$

Here a dot indicates differentiation with respect to time. The $\boldsymbol{d}$ and $\boldsymbol{\phi}_j$ are the vectors whose entries are the unknown nodal values of u in Ω and of ϕ_j on Γ_{E}, respectively. The first equation in (122) means that the entries of the vector $\boldsymbol{\phi}_0$ are equal to the entries of $\boldsymbol{d}$ for all the nodes on the boundary Γ_{E}. The element-level expressions for the arrays appearing in (120) and (121) may easily be deduced from (115) and (116):

$$M_{ab}^e=\int_{\Omega^e}N_aN_b,\,\mathrm{d}\Omega \tag{123}$$

$$C_{ab}^e=a_0c\int_{\Gamma_{\mathrm{E}}^e}N_aN_b\,\mathrm{d}\Gamma, \tag{124}$$

$$K_{ab}^e=c^2\int_{\Omega^e}\nabla N_a\cdot\nabla N_b, \tag{125}$$

$$F_a^e=\int_{\Omega^e}N_af, \tag{126}$$

$$G_{ab}^e=a_0c\int_{\Gamma_{\mathrm{E}}^e}N_aN_b^{(1)}\,\mathrm{d}\Gamma, \tag{127}$$

$$(A_j^e)_{ab}=l_{j,j-1}\int_{\Gamma_{\mathrm{E}}^e}N_a^{(j)}N_b^{(j-1)}\,\mathrm{d}\Gamma, \tag{128}$$

$$(B_j^e)_{ab}=l_{j,j}\int_{\Gamma_{\mathrm{E}}^e}N_a^{(j)}N_b^{(j)}\,\mathrm{d}\Gamma, \tag{129}$$

$$(D_j^e)_{ab} = l_{j,j+1} \int_{\Gamma_E^e} N_a^{(j)} N_b^{(j+1)} \, d\Gamma, \tag{130}$$

$$(E_j^e)_{ab} = c^2 m_{j,j-1} \int_{\Gamma_E^e} \partial_y N_a^{(j)} \partial_y N_b^{(j-1)} \, d\Gamma, \tag{131}$$

$$(H_j^e)_{ab} = c^2 m_{j,j} \int_{\Gamma_E^e} \partial_y N_a^{(j)} \partial_y N_b^{(j)} \, d\Gamma, \tag{132}$$

$$(I_j^e)_{ab} = c^2 m_{j,j+1} \int_{\Gamma_E^e} \partial_y N_a^{(j)} \partial_y N_b^{(j+1)} \, d\Gamma. \tag{133}$$

The global arrays appearing in (120) and (121) are obtained by the usual FE assembly process from the element arrays (123)–(133).

If all the shape functions $N_a^{(j)}$ are chosen to be identical, i.e. $N_a^{(j)} = \overline{N}_a$, and if in addition these boundary shape functions coincide with the trace of the domain shape functions N_a, then it is clear that many element matrices in (123)–(133) become identical up to a scaling factor. In fact, the matrices $\boldsymbol{C}^e$, $\boldsymbol{G}^e$, $\boldsymbol{A}^e$, $\boldsymbol{B}^e$ and $\boldsymbol{D}^e$ all become factors of the "boundary mass matrix" $\int_{\Gamma^e_E} \overline{N}_a \overline{N}_b \, d\Gamma$, and the matrices $\boldsymbol{E}^e$, $\boldsymbol{H}^e$ and $\boldsymbol{I}^e$ all become factors of the "boundary stiffness matrix" $\int_{\Gamma_E^e} \partial_y \overline{N}_a \partial_y \overline{N}_b d\Gamma$. Thus the calculation of the boundary element arrays becomes very efficient.

In contrast to the solution procedure adopted in [20], we do not split the system of ODEs (120) and (121) into separate subsystems (one for each j) and pass information among them by performing iterations within each time-step. Instead we solve the entire system of ODEs as a whole, in a fashion analogous to what we do in the FD scheme (Section 8.2). Thus, at each time step we do the following:

- For all unknowns associated with u values in Ω (namely for the entries of $\boldsymbol{d}$ in (120) excluding those associated with nodes on Γ_E) we step in time using an *explicit* second-order scheme (the standard central difference with a lumped mass matrix, which is the Newmark scheme with $\beta = 0$, $\gamma = 1/2$; see [32]).
- After the u values in Ω are determined at the current time-step, we solve the complete set of equations for all the $\boldsymbol{\phi}_j$ (including $\boldsymbol{\phi}_0$) for this time. From (120) and (121), the augmented system has the form

$$\boldsymbol{M}_\phi \ddot{\boldsymbol{\Phi}} + \boldsymbol{C}_\phi \dot{\boldsymbol{\Phi}} + \boldsymbol{K}_\phi \boldsymbol{\Phi} = \boldsymbol{F}_\phi. \tag{134}$$

  To solve this system, we step in time using an *implicit* second-order scheme (the average acceleration, which is the Newmark scheme with $\beta = 1/4$, $\gamma = 1/2$; see [32]).

The vector $\boldsymbol{\Phi}$ in (134) contains as entries all the ϕ_j values at node 1 on the boundary Γ_E, then all the ϕ_j values at node 2 on the boundary, etc. The matrices $\boldsymbol{M}_\phi$, $\boldsymbol{C}_\phi$ and $\boldsymbol{K}_\phi$ are of dimension $N_\phi = (P+1)N_{\Gamma_E}$ where N_{Γ_E} is the number of nodes on the boundary Γ_E. These matrices are all sparse; their maximal bandwidth can be shown to be $4P+3$. These matrices are not symmetric, but they are well behaved. (The motivation to work iteratively in [20] was to keep all matrices symmetric.) As an example we consider the structure of the element matrix $\boldsymbol{M}_\phi^e$, which is the element-level counterpart of $\boldsymbol{M}_\phi$. We give here the expression for the entry $(M_\phi^e)_{(ai)(bj)}$ of the matrix $\boldsymbol{M}_\phi^e$, which is the entry associated with the equation parameterized by node a of the boundary element ($a = 1, 2$) and auxiliary variable i ($i = 0, \ldots, P$) and with the unknown parameterized by node b of the boundary element ($b = 1, 2$) and auxiliary variable j ($j = 0, \ldots, P$):

$$(M_\phi^e)_{(ai)(bj)} = \begin{cases} M_{ab}^e; & i = j = 0 \\ (A_i^e)_{ab}; & j = i-1, \ i \neq 0 \\ (B_i^e)_{ab}; & j = i, \ i \neq 0 \\ (D_i^e)_{ab}; & j = i+1, \ i \neq 0 \\ 0; & \text{otherwise} \end{cases} \tag{135}$$

The matrix $\boldsymbol{K}^e_\phi$ has an analogous structure. The matrix $\boldsymbol{C}^e_\phi$ is defined as

$$(C^e_\phi)_{(ai)(bj)} = \begin{cases} C^e_{ab}; & i = j = 0 \\ -C^e_{ab}; & i = 0,\ j = 1 \\ 0; & \text{otherwise} \end{cases} \tag{136}$$

The right-side vector $\boldsymbol{F}_\phi$ involves known values of u in the "layer of nodes" immediately adjacent to the boundary Γ_{E}.

8.2. Finite difference scheme

We have also implemented a high-order (in practice the code is capable of stable computations up to about 20th order) difference approximation to the wave equation coupled with the boundary system. Assuming a uniform grid away from the boundaries, spatial derivatives are approximated to order $2q$ by the standard central difference formulas with $2q$-point stencils [35]. Near boundaries we replace these by order $2q$ one-sided approximations with $2q+2$-point stencils. On the uniform grid these would be unstable. They are stabilized via the introductions of a small number (1–3) of additional subcell nodes near the boundaries. Here we have used 8th order discretizations on the grids constructed in [36] with two subcell nodes near each boundary. We note that the grids used are optimized for first order systems; analogous constructions for second order problems are underway [37]. Precisely the same approximations are used for the boundary system.

Introduction of the grids and the difference approximations leads to a semidiscrete system of the form:

$$\frac{\mathrm{d}^2 U_i}{\mathrm{d}t^2} = (GU)_i + F_i, \quad \boldsymbol{x}_i \in \text{Interior}, \tag{137}$$

$$L\frac{\mathrm{d}^2 \boldsymbol{\Phi}_i}{\mathrm{d}t^2} = M(G\boldsymbol{\Phi})_i + S\boldsymbol{\Phi}_i + \left(m_{10}(GU)_i - l_{10}\frac{\mathrm{d}^2 U_i}{\mathrm{d}t^2}\right)\mathbf{e}_1, \quad \boldsymbol{x}_i \in \text{Artificial boundary}, \tag{138}$$

$$a_0\frac{\mathrm{d}U_i}{\mathrm{d}t} + c(DU)_i = a_0\frac{\mathrm{d}\Phi_{1,i}}{\mathrm{d}t}, \quad \boldsymbol{x}_i \in \text{Artificial boundary}. \tag{139}$$

Here G denotes the order $2q$ difference approximation to the Laplacian and D a one-sided, order $2q$ approximation to the outward normal derivative. We also assume that unknowns associated with nodes on the physical boundaries have been removed using the boundary conditions.

Time marching of the semidiscrete system is accomplished using an order s Taylor series applied to a first order reformulation. In particular if we introduce a time step Δt and scaled first derivatives:

$$V_i = \Delta t\frac{\mathrm{d}U_i}{\mathrm{d}t}, \ \mathbf{W}_i = \Delta t\frac{\mathrm{d}\boldsymbol{\Phi}_i}{\mathrm{d}t}, \tag{140}$$

one obtains a system of the form:

$$\frac{\mathrm{d}\mathbf{Z}}{\mathrm{d}t} = \frac{1}{\Delta t}H\mathbf{Z}, \tag{141}$$

where $\mathbf{Z}$ contains all the unknowns on the grid (including the scaled time derivatives). (For simplicity we have assumed $F_i = 0$, though nonzero forcings can be incorporated into the method). Note that the matrix H is quite sparse. It consists of difference operators, the banded matrices M and S, as well as multiplications by L^{-1}. An analogous reduction of the finite element system would not be sparse due to the mass matrix. Then we approximate:

$$\mathbf{Z}(t+\Delta t) = \sum_{j=0}^{s}\mathbf{Z}^{(j)}, \tag{142}$$

where

$$\mathbf{Z}^{(j)} = \frac{1}{j}H\mathbf{Z}^{(j-1)}, \quad \mathbf{Z}^{(0)} = \mathbf{Z}(t). \tag{143}$$

In the following experiments we choose $2q = s = 8$. Note that for the layer problem each layer is gridded and discretized independently with an enforcement of the continuity conditions at the interface used to update the interface variables.

9. Numerical examples

In the following subsections we present some numerical experiments using either the FD or FE scheme or both. One should recall the following two facts:

- The FD scheme used here is of high order (8th order in the examples shown) in space and time (see Section 8.2) whereas the standard h-version FE scheme used is second order in space and time.
- The discretization error is reduced algebraically when the discretization is refined, whereas the error due the boundary condition decreases exponentially fast with the ABC order P or $P+E$, as we have shown.

Thus, for a given time and space discretization the total error is reduced with increasing P in both the FD and FE schemes until it reaches the discretization error level, at which point no further reduction in the error is possible unless the discretization is refined. The value of the ABC order P for which this occurs is much lower in the FE scheme (typically $P = 4$ for the examples shown here) than in the FD scheme. Moreover, for a given discretization in space and time the high-order FD scheme is expected in general to be much more accurate than the FE scheme. Of course, replacing the standard FE scheme by a high-order FE method (p-version or spectral elements) is bound to eliminate this limitation in accuracy.

9.1. Homogeneous non-dispersive medium, propagating waves

We start with a wave guide containing a homogeneous non-dispersive medium. We begin by setting $b = 3$ and $c = 1$. Unless otherwise indicated we take $u_W \equiv 0$ in (3). We solve two problems with these parameters using the FE method. In the first we synthesize a problem whose solution is the analytic "wave-guide mode"

$$u(x,y,t) = \cos\left(\frac{n\pi y}{b}\right)\cos(kx - \omega t), \tag{144}$$

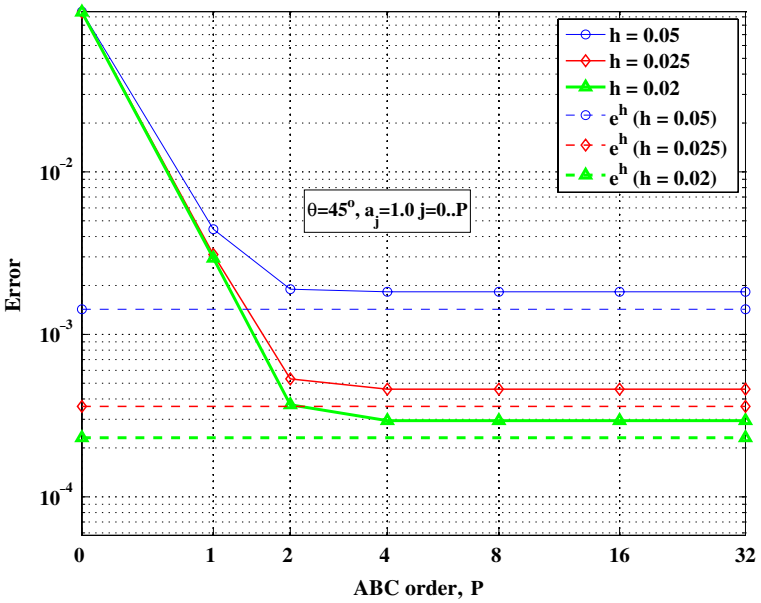

Fig. 4. The "wave-guide mode" problem, homogeneous non-dispersive medium, $\theta = 45°$: the $L_2(\Gamma_E)$ error averaged over one time-period as a function of the ABC order P, for three different meshes. Also shown (in dashed lines) are the levels of discretization error corresponding to the three meshes.

where the dispersion relation is

$$\omega^2 = c^2\left[\left(\frac{n\pi}{b}\right)^2 + k^2\right], \tag{145}$$

and the incident angle θ is given by

$$\cos\theta = kc/\omega. \tag{146}$$

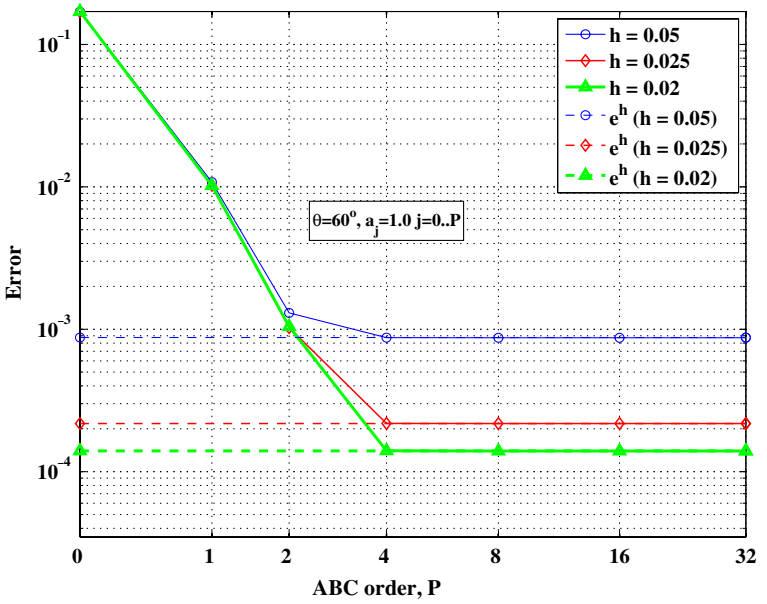

Fig. 5. The "wave-guide mode" problem, homogeneous non-dispersive medium, $\theta = 60°$: the $L_2(\Gamma_E)$ error averaged over one time-period as a function of the ABC order P, for three different meshes. Also shown (in dashed lines) are the levels of discretization error corresponding to the three meshes.

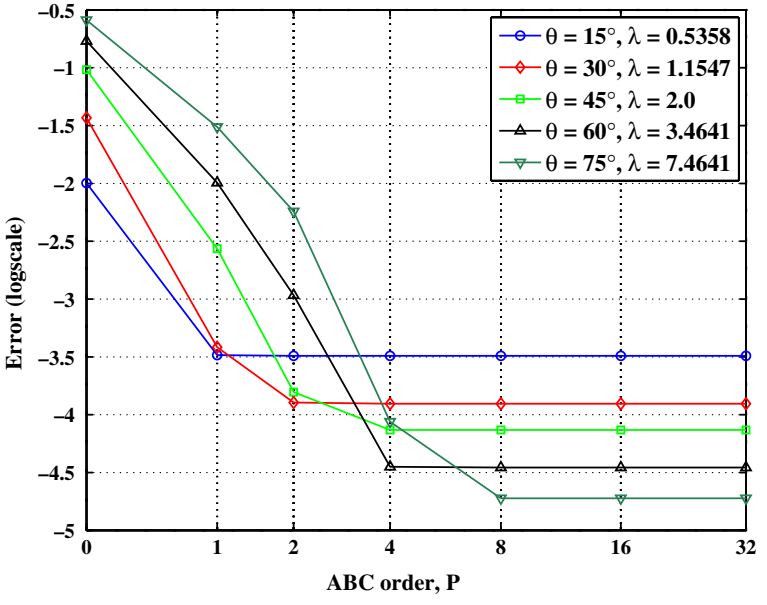

Fig. 6. The "wave-guide mode" problem, homogeneous non-dispersive medium, mesh with $h = 0.01$: the $L_2(\Gamma_E)$ error averaged over one time-period as a function of the ABC order P, for different angles of incidence.

We set $n = 3$ and either $k = \pi$, which gives $\omega = \sqrt{2}\pi$ and $\theta = 45^\circ$, or $k = \pi/\sqrt{3}$, which gives $\omega = 2\pi/\sqrt{3}$ and $\theta = 60^\circ$. The west boundary function u_W (see (3)) and all the initial condition values (including the initial values of the ϕ_j) are set according to the analytic solution (144). The computational domain is the square $\Omega = [0,3] \times [0,3]$.

We use a uniform mesh with bilinear square elements and consider various mesh densities. Namely we vary the mesh parameter h (the element size), while setting the time-step size Δt so as to maintain $c\Delta t/h = \sqrt{2}/2$. (This value of the Courant number is optimal in terms of dispersion error in one dimension; see [38].) Fig. 4 shows, for $\theta = 45^\circ$, the $L_2(\Gamma_E)$ error averaged over one time-period that is generated by the FE scheme, as a function of the ABC order P. This error is shown for three different meshes. Also shown (in dashed lines) are the levels of discretization error corresponding to the three meshes, when no domain truncation is involved. These discretization errors were estimated by comparing the analytic solution (144) to a FE solution obtained in a long domain and with the same mesh density. Fig. 5 shows similar results for $\theta = 60^\circ$. It is apparent that the total error decreases as P increases until it approximately reaches the discretization error level. In the case

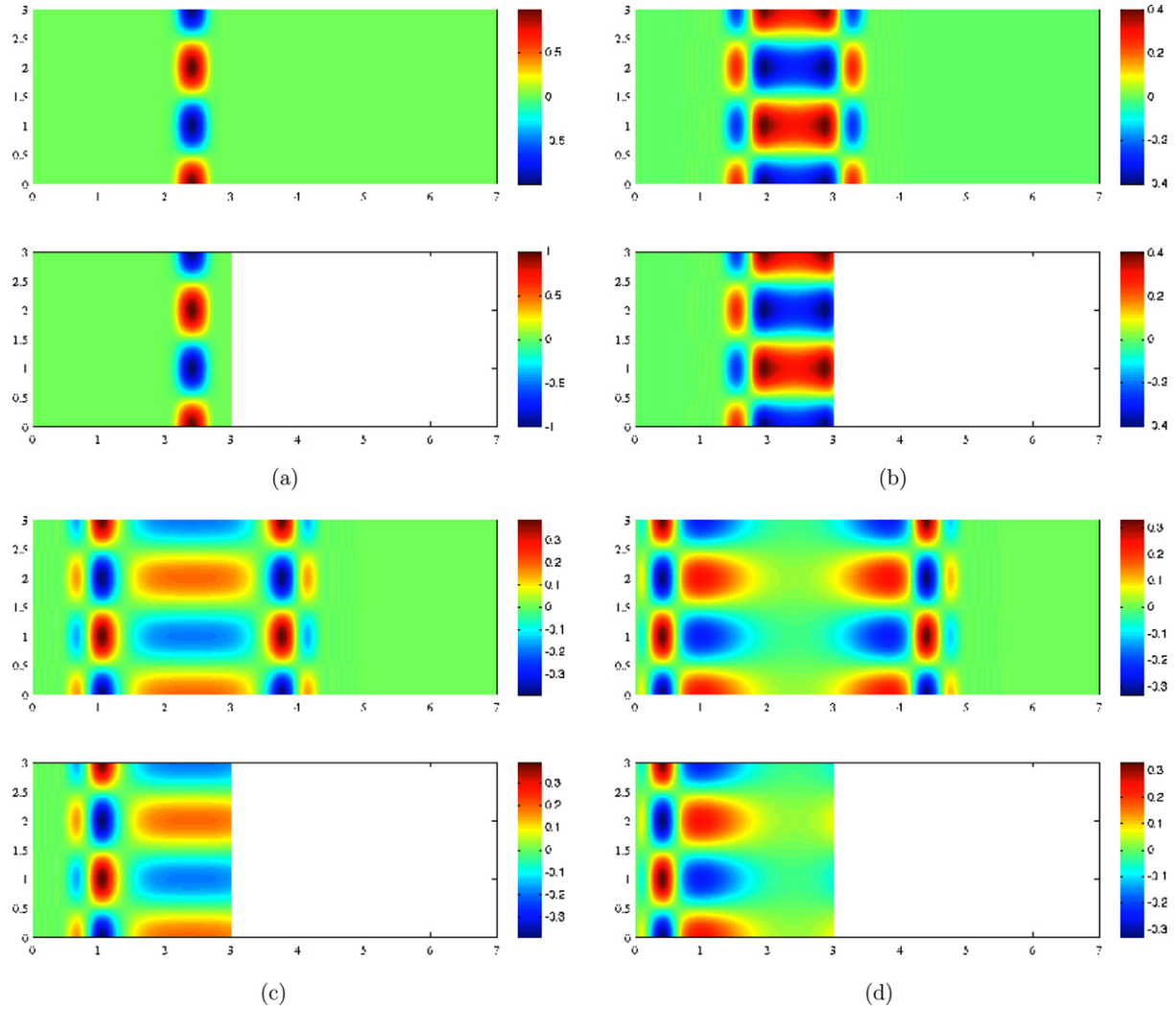

Fig. 7. The compact initial datum problem, homogeneous non-dispersive medium, $c = 2$: solution color-map snapshots. For each time, the computational solution (lower of each pair) is compared to a reference solution in a long domain (upper of each pair). Solutions are shown at times: (a) $t = 0$, (b) $t = 0.397$, (c) $t = 0.804$, and (d) $t = 1.096$.

$\theta = 45^\circ$ the total errors converge to a value slightly about the discretization error, while for $\theta = 60^\circ$ the limit total error value practically coincides with the discretization error.

Fig. 6 shows, for a mesh with $h = 0.01$, the error as a function of P for different angles of incidence. It is important to realize that in the case of wave-guide modes, as opposed to plane waves in free space, the angle of incidence θ is not independent of the wave lengths λ and μ in the x and y directions, respectively. The dependence between θ, λ and μ is given by (146) and (145) where $\lambda = 2\pi/k$ and $\mu = 2b/n$. For the mode we consider here we take $n = 3$; thus setting a certain value for θ implies also setting a value for k or λ. We note that it is impossible to take $\theta = 0$, namely normal incidence, for $n \neq 0$, since in that case $k \to \infty$. This is very different than the situation for plane waves in free space, where normal incidence is regarded as the most basic benchmark to be considered.

According to Fig. 6, the error for a sufficiently large P decreases as the angle of incidence becomes more oblique. At first sight this looks surprising, since one may expect quite the opposite to happen. However, note that for a smaller angle θ one obtain a smaller wave length λ, and hence the resolution that the mesh provides (i.e. number of elements per wave-length and number of time-steps per period) deteriorates. This immediately implies that the discretization error is larger when the angle of incidence is smaller. The total error cannot be much lower than the discretization error, even if the ABC error alone becomes smaller for small angles.

We also note from Fig. 6 that the error decreases (to the discretization error) with increasing P *faster* for small angles of incidence. This is caused by the fact that we work with the Padé ABC coefficients, i.e. $a_j = 1$, which become optimal for angles of incidence close to normal.

The second example concerns initial data (see (5)) of compact support. We set the initial velocity v_0 to zero, while u_0 is defined by

$$u_0(x,y) = \begin{cases} \cos(\pi y)\frac{64(x-2)^3(2.8-x)^3}{0.8^6}, & 2.0 \leqslant x \leqslant 2.8 \\ 0, & \text{otherwise} \end{cases} \tag{147}$$

The sixth-order polynomial in x appearing here was chosen so that $u_0 \in C^1(\Omega)$, namely it rises smoothly from the value 0 to the value 1 and back to 0. The computational domain is the square $[0,3] \times [0,3]$. The other parameters are the same as in the previous example. We solve this problem using the FE scheme. Since an

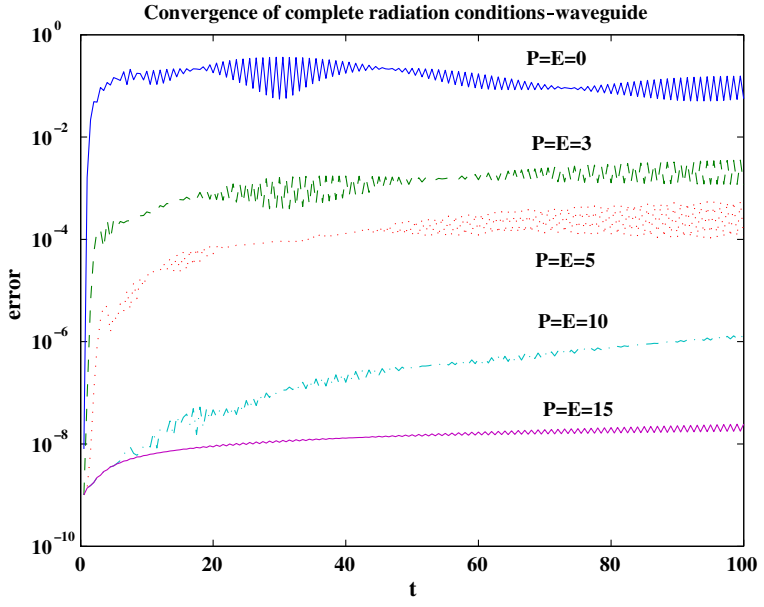

Fig. 8. The Gaussian initial datum problem, homogeneous non-dispersive medium: the L_2 error in space as a function of time for various P and E values.

analytic solution corresponding to the given initial data is difficult to obtain, we generate a reference solution by solving the problem using the same FE scheme in the much longer domain $[0, 8] \times [0, 3]$.

The L_2 error curves behave similarly to those in the previous example. Here we show snapshots of the solution obtained with $h = 0.02$ (22,500 elements in the truncated domain and 60,000 elements in the reference

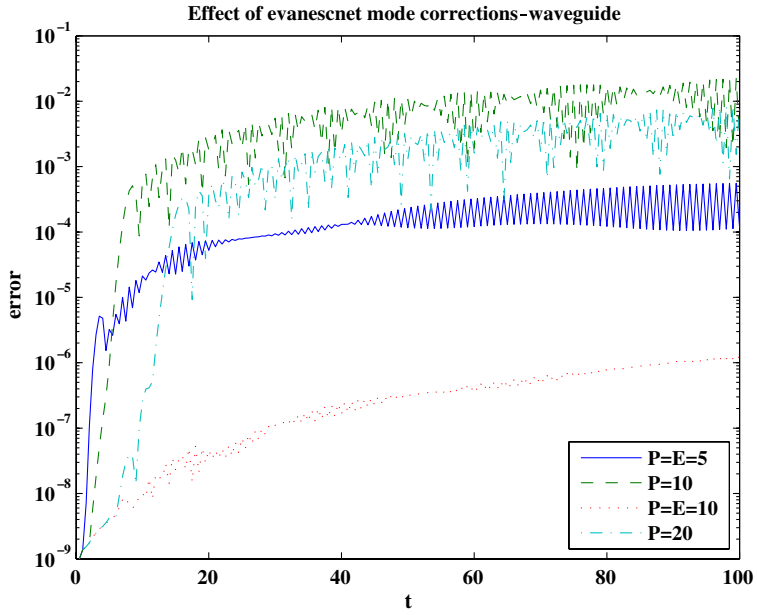

Fig. 9. The Gaussian initial datum problem, homogeneous non-dispersive medium: comparison of the L_2 error in space as a function of time with and without evanescent mode corrections.

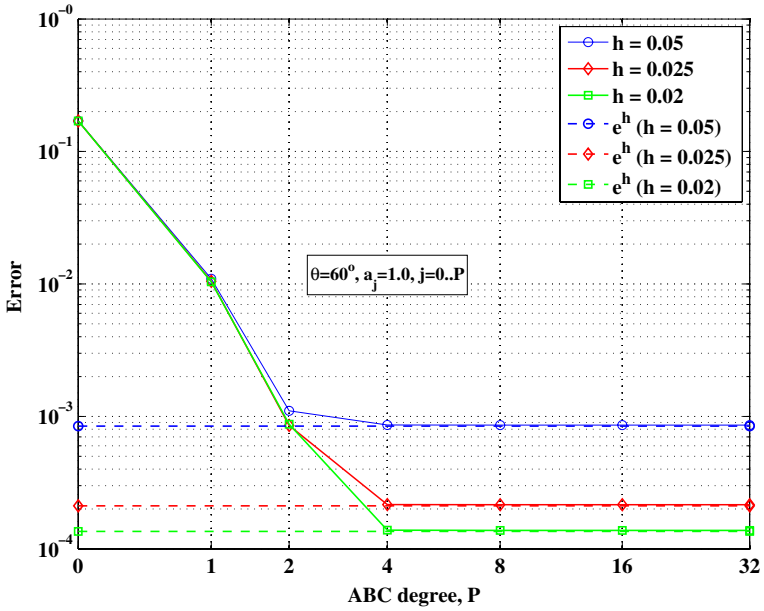

Fig. 10. The "wave-guide mode" problem, dispersive medium, $f = 1$, $\theta = 60°$: the $L_2(\Gamma_E)$ error averaged over one time-period as a function of the ABC order P, for three different meshes. Also shown (in dashed lines) are the levels of discretization error corresponding to the three meshes.

domain) and $P = 5$. Fig. 7 shows the color map of the solution at times $t = 0$, 0.397 (when the wave fronts just passed through the east boundary), 0.804 and 1.096. For each time, the computational solution (lower of each pair) is compared to the reference solution in the long domain (upper of each pair). The excellent agreement between the two solutions is apparent.

The third example involves a Gaussian initial condition in a wave guide. The exact solution corresponds to a space-time Gaussian source with variance 35 centered at $t = -0.95$, $x = 0.05033$, $y = 1/2$ with image sources determined to satisfy Dirichlet boundary conditions on the walls. That is:

$$u(x,y,t) = \sum_{k=-\infty}^{\infty} (\pm) \int_{-\infty}^{t-r_k} ((t-s)^2 - r_k^2)^{-1/2} \exp(-35(s+0.95)^2)\, ds, \tag{148}$$

where r_k is the distance from (x,y) to the kth image source and the signs are chosen to enforce the Dirichlet conditions

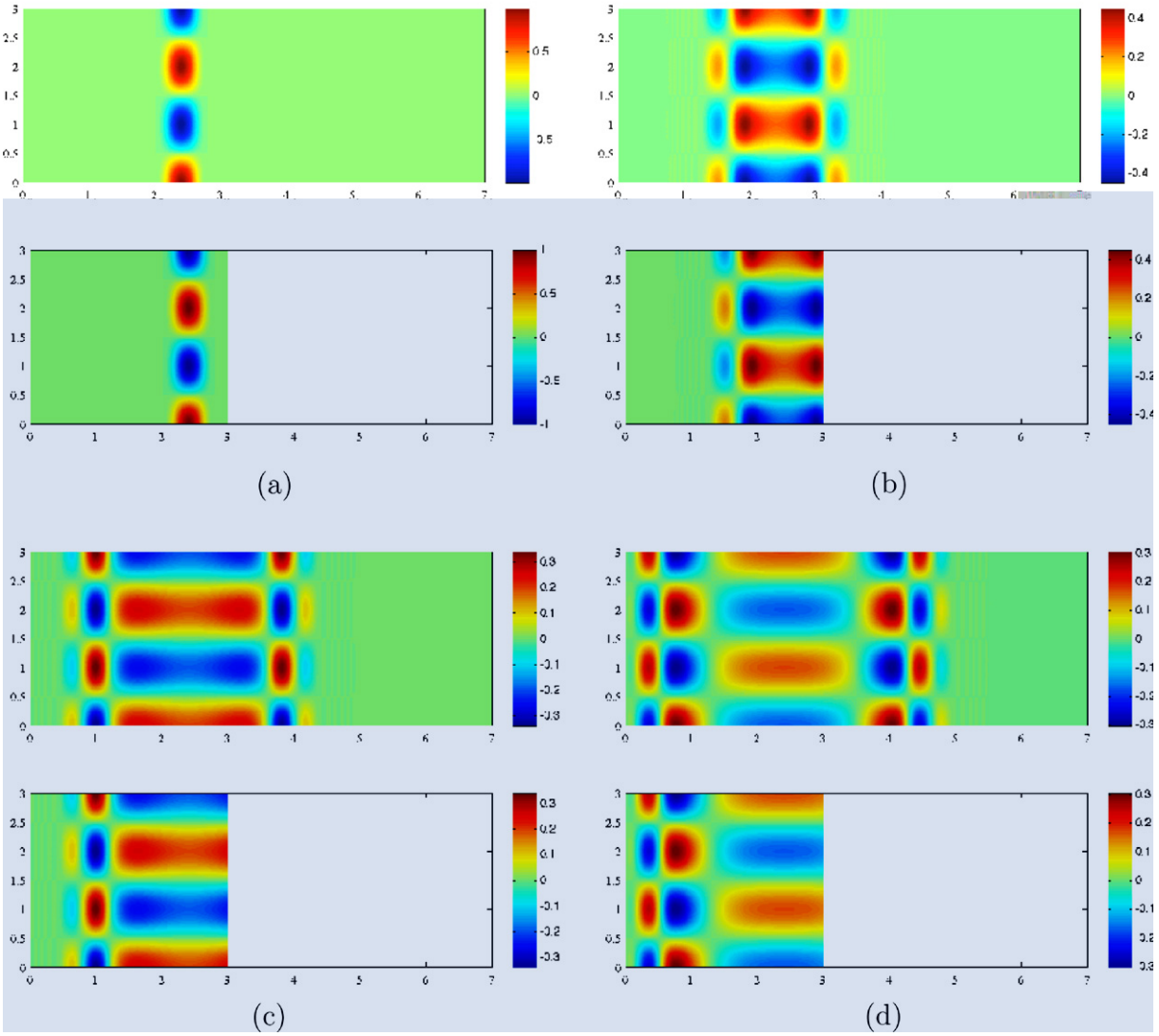

Fig. 11. The compact initial datum problem, dispersive medium, $c = 2$, $f = 4$: solution color-map snapshots. For each time, the computational solution (lower of each pair) is compared to a reference solution in a long domain (upper of each pair). Solutions are shown at times: (a) $t = 0$, (b) $t = 0.397$, (c) $t = 0.804$, and (d) $t = 1.096$.

$$u = 0, \quad y = 0, 1. \tag{149}$$

We solve this problem with the high-order FD scheme. Fig. 8 shows the L_2 error in space as a function of time for various boundary condition orders and with $P = E$. (The initial L_2-norm of the solution is $O(1)$ so these are comparable to relative errors.) Here the parameters for both the P and E terms are chosen according to the quadrature rules described in Section 7.1. We take $\delta = 1$, deliberately avoiding the optimal choice based on the source location, $\delta \approx 2$. (Choosing $\delta = 2$ led to only slight improvements.) The computational domain is taken to be $[-2, 2] \times [0, 1]$ with the absorbing boundary conditions applied at both ends and we take $\Delta x = \Delta y = \frac{1}{75}$ and $\Delta t = \frac{1}{750}$.

Clearly, we observe exponential convergence with increasing order with very little long time error growth. Extreme accuracy is achieved for $P = E = 15$ while even for $P = E = 3$ the long time error remains below 0.35%.

We also compare these results with results obtained using only P terms in the boundary condition; see Fig. 9. For a fixed total number of auxiliary functions, the P-only conditions are more accurate for short times but considerably less accurate as t grows. This is consistent with the theory developed in [27].

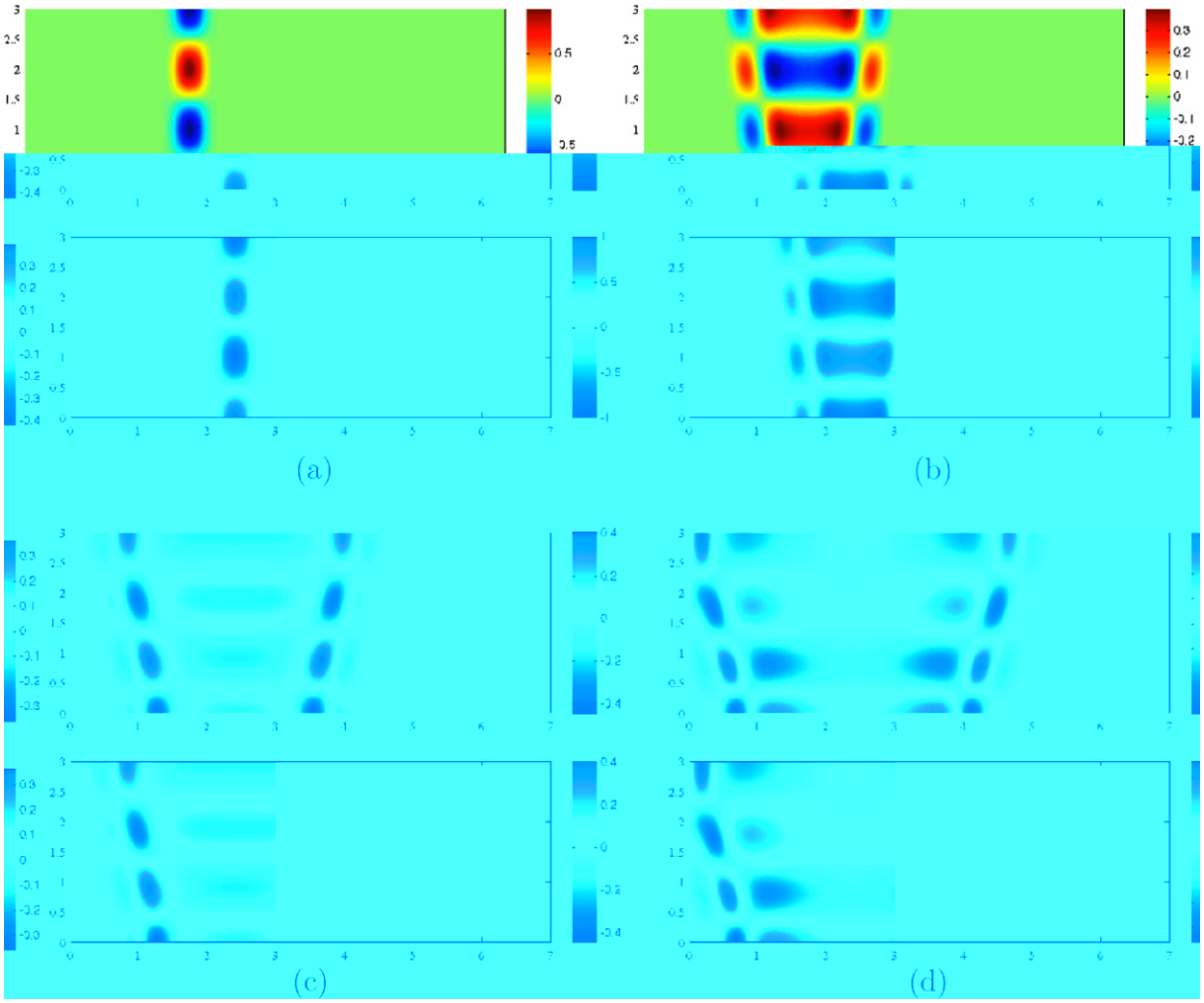

Fig. 12. The compact initial datum problem, non-dispersive medium, wave-speed varies linearly in the cross-section, with average 2 and slope $\alpha = 0.2$: solution color-map snapshots. For each time, the computational solution (lower of each pair) is compared to a reference solution in a long domain (upper of each pair). Solutions are shown at times: (a) $t = 0$, (b) $t = 0.397$, (c) $t = 0.804$, and (d) $t = 1.096$.

9.2. Dispersive medium

Now we reconsider the first two examples presented in the previous section, but now we include a dispersion term in the wave equation; see (61). We set the value of the dispersion parameter to $f = 1$. We show only FE results.

The wave-guide mode solution (144) remains unchanged, but the dispersion relation (145) becomes

$$\omega^2 = c^2\left[\left(\frac{n\pi y}{b}\right)^2 + k^2\right] + f^2. \tag{150}$$

The error curves turn out to be very similar to those in the non-dispersive case. For example, compare Fig. 10, which shows the error in the case $\theta = 60^\circ$, with Fig. 5.

Fig. 11 shows the solution snapshots for $f = 4$, and should be compared with Fig. 7 for the non-dispersive case. Due to the dispersion effect, the waves are now less local in nature, and the wave fronts moving to the left and right are much less separated. Again, the computational and reference solutions agree very well.

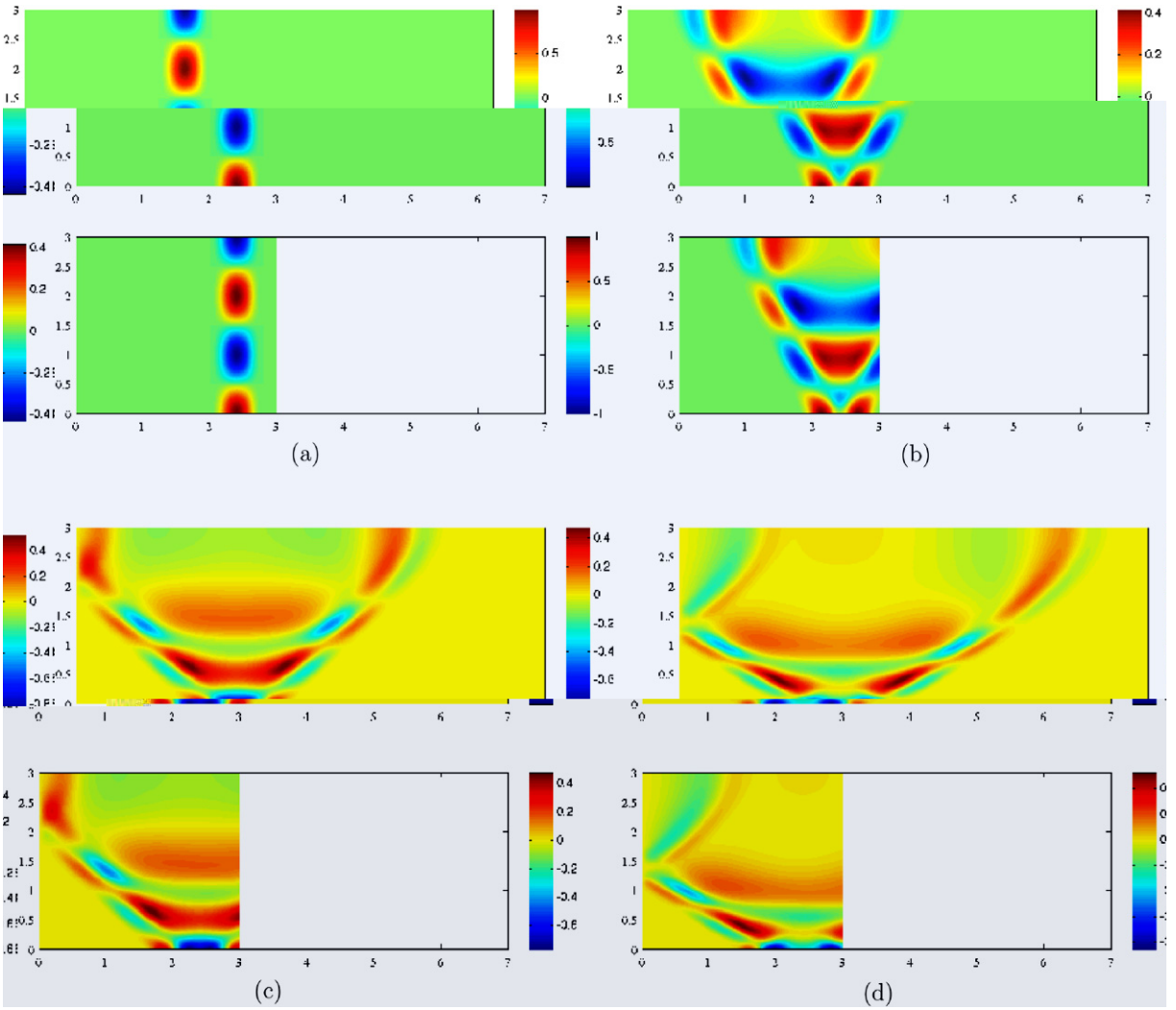

Fig. 13. The compact initial datum problem, non-dispersive medium, wave-speed varies linearly in the cross-section, with average 2 and slope $\alpha = 1.0$: solution color-map snapshots. For each time, the computational solution (lower of each pair) is compared to a reference solution in a long domain (upper of each pair). Solutions are shown at times: (a) $t = 0$, (b) $t = 0.397$, (c) $t = 0.804$, and (d) $t = 1.096$.

9.3. Linearly-varying wave speed

Now we let the wave speed c vary linearly in the cross-section, i.e. $c(y) = \alpha y + \beta$. The following results were obtained with the FE scheme. We calculate all the FE arrays by *exactly* evaluating the relevant integrals (see Section 8.2) involving the function $c(y)$.

Here we consider the compact initial datum problem as described in Section 9.1. We set $f = 0$ (non-dispersive medium). We fix the average wave speed in the cross-section at 2.0, and vary α, the slope of $c(y)$. The wave speed increases with y, namely it is larger at the top of the wave guide than at the bottom. Figs. 12 and 13 show snapshots of the solution for $\alpha = 0.2$ and $\alpha = 1$, respectively. The effect of the varying wave speed is prominent. In both cases the agreement between the computational and reference solutions is quite good.

For the wave-guide mode problem, Fig. 14 depicts the L_2 error as a function of the wave-speed slope α for various values of the ABC order P. As in the homogeneous medium case, the error decreases with increasing P until it reaches the discretization error level. The latter is almost constant for $0 \leqslant \alpha \leqslant 0.6$ and then increases with increasing α.

We now combine the effects of varying wave speed and dispersion, and set $\alpha = 1$ and $f = 4$. Fig. 15 shows the snapshots of the solution. Despite the very rich content of the wave field, the agreement between the computational and reference solutions is satisfactory in this case too.

9.4. Layers

We now use the finite difference method with the same mesh spacings and time steps as in Section 9.1. Now the domain is $[-2, 2] \times [-1, 1]$, divided into two horizontal layers of equal width, whose wave speeds are $c = 1$ and $c = 2$. Homogeneous Dirichlet conditions are imposed on $y = \pm 1$. Initial data are $u = 0$ and

$$\frac{\partial u}{\partial t}(x, y, 0) = 25\mathrm{e}^{-50(x^2+(y-0.9)^2)} - 25\mathrm{e}^{-50(x^2+(y-1.1)^2)}. \tag{151}$$

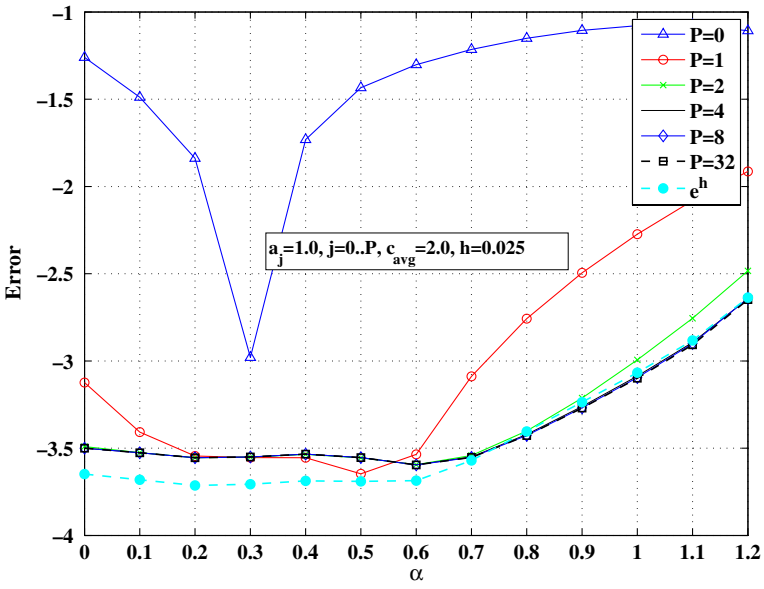

Fig. 14. The wave-guide mode problem, non-dispersive medium, wave-speed varies linearly in the cross-section, with average 2 and slope α: the $L_2(\Gamma_E)$ error as a function of α for various values of the ABC order P.

As a reference solution we use the solution obtained using the same FD scheme in a much longer domain, $[-32, 32] \times [-1, 1]$ up to $t = 30$ and with the same discretization in space and time. (As the Gaussian is somewhat sharper these calculations are less well resolved than those presented in Section 9.1.)

Fig. 16 shows the L_2 error in space as a function of time for various P and E values as well as two choices for c_0. We see that the results again display exponential convergence. The error behavior is essentially uniform in time with the exception of the highest order conditions. For these we believe we are encountering the effects of discretization error for t large. Overall, the best performance is obtained with $P = E$ and $c_0 = 2$, though certainly all our parameter choices led to excellent accuracy at low cost.

In Fig. 17 we compare contour plots of the long domain solution and two truncated domain solutions: one with $P = E = 0$ (Sommerfeld condition) and one with $P = E = 6$ and $c_0 = 2$. Clearly, the latter is indistinguishable from the long domain solution while use of the Sommerfeld condition leads to obvious reflections.

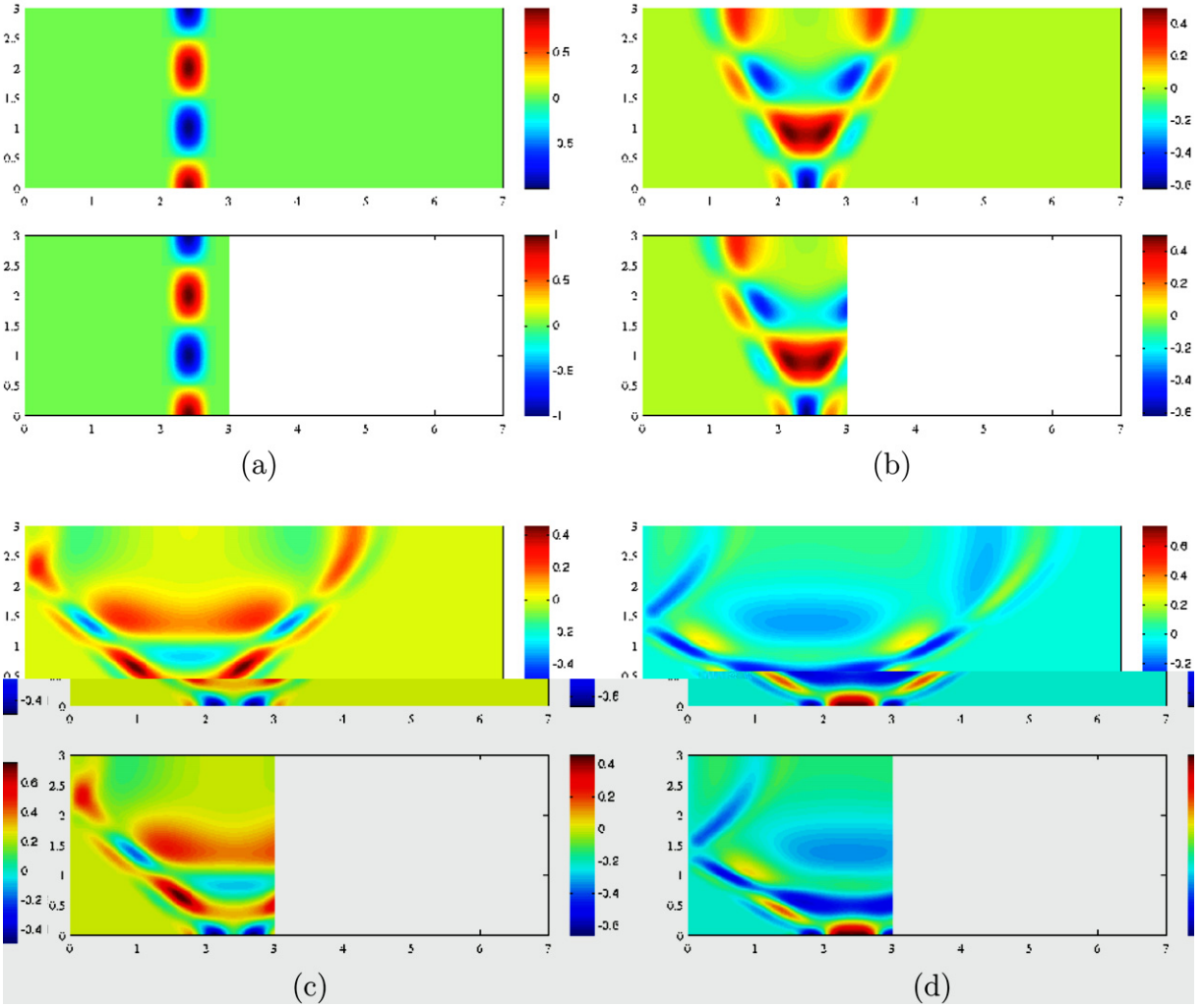

Fig. 15. The compact initial datum problem, a dispersive non-homogeneous medium, wave-speed varies linearly in the cross-section, with average 2 and slope $\alpha = 1.0$, dispersion parameter $f = 4$: solution color-map snapshots. For each time, the computational solution (lower of each pair) is compared to a reference solution in a long domain (upper of each pair). Solutions are shown at times: (a) $t = 0$, (b) $t = 0.397$, (c) $t = 0.804$, and (d) $t = 1.096$.

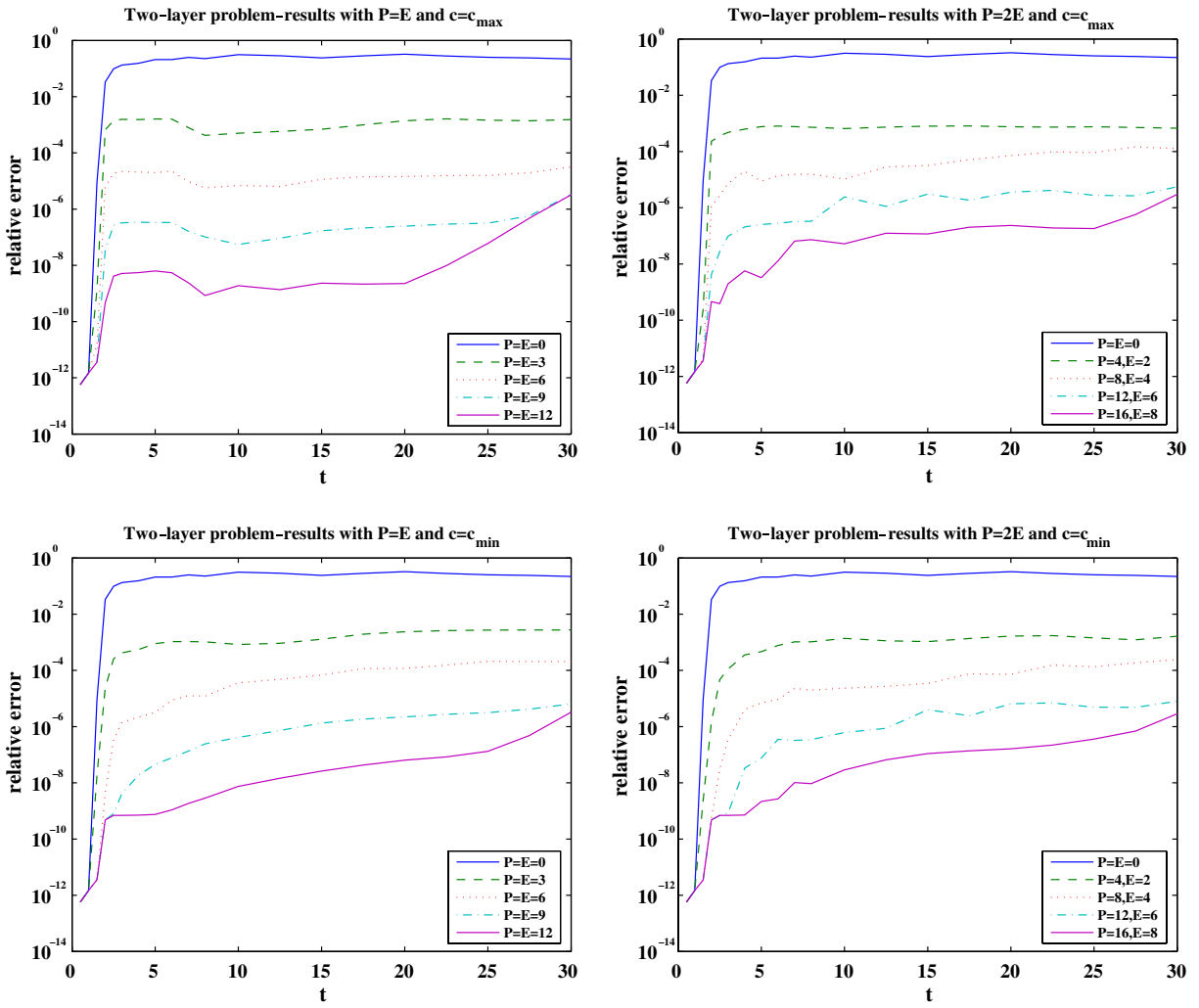

Fig. 16. The Gaussian initial datum problem, double-layer medium: the L_2 error in space as a function of time for various E and P values and two choices for c_0.

9.5. Evanescent modes

The previous examples with the finite difference method demonstrate the effectiveness of the evanescent mode corrections. Here we carry out FE calculations specifically designed to assess the treatment of these modes. We consider a homogeneous non-dispersive medium, as in Section 9.1, including the evanescent modes in the ABC.

First we synthesize an analytic solution which consists of the single "wave-guide evanescent mode"

$$u(x,y,t) = \exp(-\sigma x)\cos(n\pi y/b)\cos(\omega t), \tag{152}$$

with the dispersion relation

$$\omega^2 = c^2\left[\left(\frac{n\pi y}{b}\right)^2 - \sigma^2\right]. \tag{153}$$

We set $c = 1$, $b = 3$, $n = 3$ and $\sigma = 1$. We apply the FE scheme with $P = 2$ and a varying number of evanescent auxiliary variables, E. All the boundary and initial conditions (including the initial conditions for the ϕ_j) are

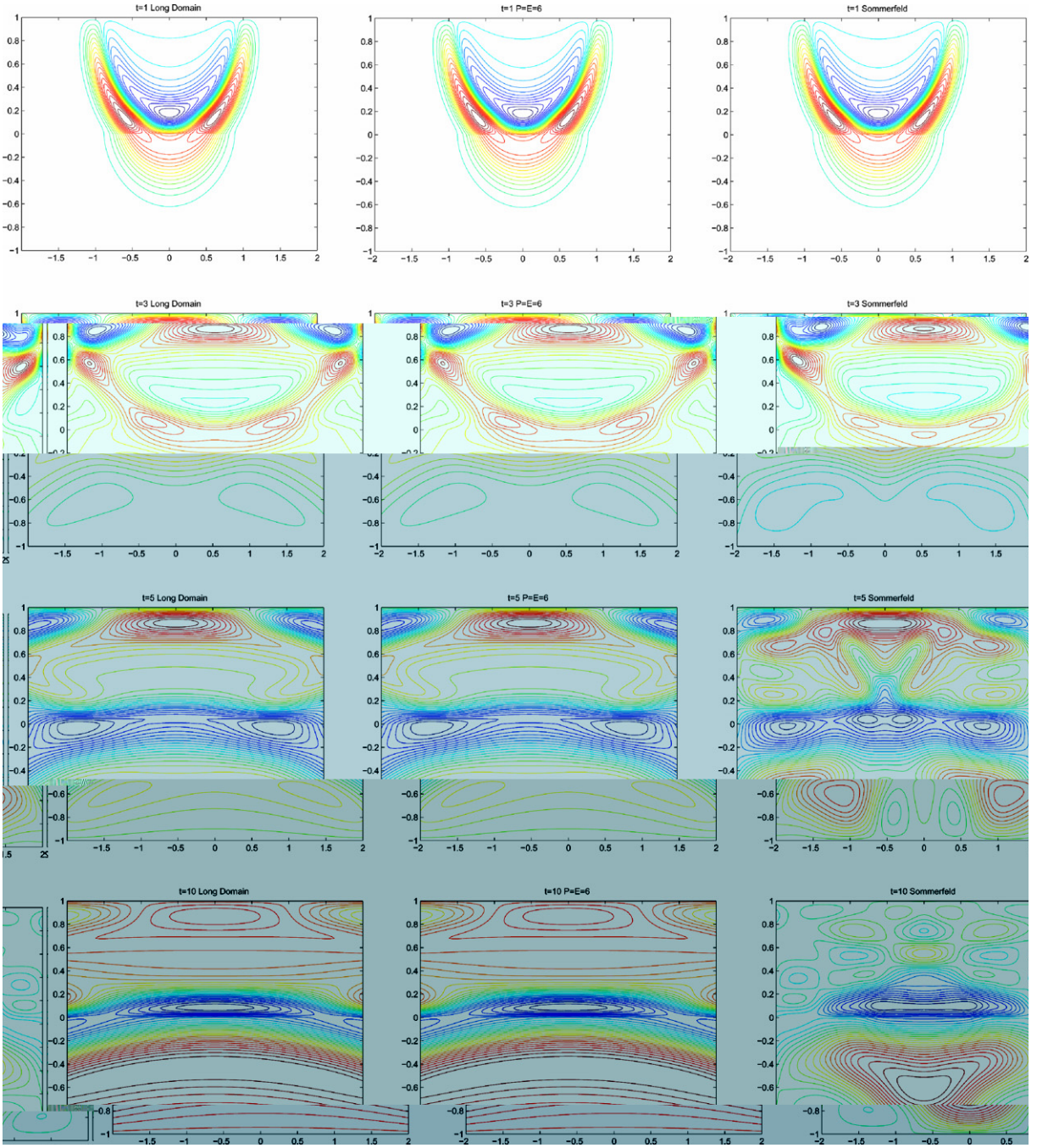

Fig. 17. The Gaussian initial datum problem, double-layer medium: comparison of the long domain solution and truncated domain solutions using zero (Sommerfeld) and twelve auxiliary functions.

set such as to correspond to the analytic solution (152). We take $a_j = 1$ for the propagating terms in the ABC and all the evanescent parameters $\sigma_j = \sigma_1$ to be equal. Fig. 18 shows the space-time L_2 error as a function of σ_1 for $E = 1, 2, 3, 4$. For $\sigma_1 = \sigma = 1$ the error is practically zero (more precisely it is equal to the discretization error), whereas when $\sigma_1 \neq \sigma$ an error is observed, which decreases with increasing order E of the ABC. This result is consistent with our analysis in Section 7.2.

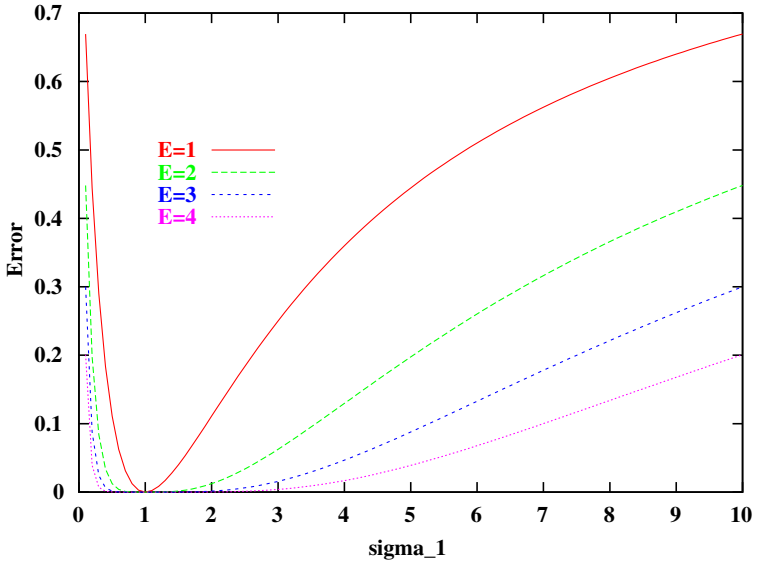

Fig. 18. The "wave-guide evanescent mode" problem, $\sigma = 1$: the space-time L_2 error as a function of the evanescent ABC parameter $\sigma_j = \sigma_1$, for different ABC orders E.

10. Concluding remarks

We have presented a number of extensions to the formulation of absorbing boundary conditions (ABC) suggested in [19], which is itself a modification of the Higdon ABC written in high order form. The extensions include the ability to use the ABC for inhomogeneous and dispersive media, as well as taking into account directly evanescent modes in the exact solution.

These extensions are crucial in the process of turning the proposed ABC into a practical powerful tool in regional simulations ("limited-area models") in fields like oil exploration, earthquake engineering, underwater acoustics and weather prediction. However, the way to achieving such a level of practicality is still very long. In particular, appropriate ABCs should be constructed for anisotropic media, analogous ABCs should be developed for more complicated governing equations, like the equations of linear anisotropic elasticity and Maxwell's equations. Also, efficient handling of corner conditions (see [19,20] and references therein) has to be further developed. For FE applications, the ABC should be incorporated in high-order FE formulations (p-version or spectral elements) in order to fully exploit the high accuracy achieved with increasing ABC orders. In addition, for applications in weather prediction and oceanography, the ABC must be turned into an "open boundary condition" which allows not only free passage of waves from the computational domain Ω outside, but also passage into Ω of waves incoming from the exterior. Extension to three dimensional geometry is also very important. In principle this extension should be straight forward, but of course it is significantly more involved technically than the two-dimensional case. We hope to report about progress in some of these directions in a future publication.

Finally, it would be insightful to compare the performance and relative cost-effectiveness of the proposed high-order ABCs to that of the perfectly matched layer (PML). We feel that there two types of methods have emerged in recent years as the dominating techniques for unbounded-domain problems, and those which currently hold the most promise for the future [1]. A comprehensive and very careful comparison between them, in the time domain, requires major work which is very much called for.

Acknowledgment

This work was supported by the US–Israel Binational Science Foundation (BSF), Research No. 2002019. T.H. was also supported, in part, by ARO Grant DAAD19-03-1-0146 and NSF Grant DMS-0610067. Any

opinions, findings, and conclusions or recommendations expressed in this paper are those of the authors and do not necessarily reflect the views of ARO or NSF. D.G. thanks Dr. Naomi Shaked-Monderer for helpful discussions.

Appendix A. The ABC truncation error as $P \to \infty$

The linear system (56) may be solved for $\eta_1^{(P)}$ using Cramer's rule:

$$\eta_1^{(P)} = |\, \boldsymbol{B}_P \,| \,/\, |\, \boldsymbol{A}_P \,|, \tag{A.1}$$

where $|\cdot|$ denotes the determinant of a matrix, $\boldsymbol{A}_P$ is the $P \times P$ matrix appearing in (56) and $\boldsymbol{B}_P$ is the same matrix but with the first column replaced by the right-side vector of (56). Let us also define the $P \times P$ Toeplitz matrix $\boldsymbol{D}_P$ as the same as matrix $\boldsymbol{A}_P$ but with the (1,1) entry $4 - S$ replaced by $4 - 2S$. Then a direct calculation gives

$$|\, \boldsymbol{A}_P \,| = (4 - S)\,|\, \boldsymbol{D}_{P-1} \,| - S^2\,|\, \boldsymbol{D}_{P-2} \,|, \quad |\, \boldsymbol{B}_P \,| = 2S\,|\, \boldsymbol{D}_{P-1} \,|\,. \tag{A.2}$$

Hence from (A.1)

$$\eta_1^{(P)} = \frac{2S}{4 - S - S^2\,|\, \boldsymbol{D}_{P-2} \,| \,/\, |\, \boldsymbol{D}_{P-1} \,|}. \tag{A.3}$$

Generally, if the $n \times n$ matrix $\boldsymbol{d}_n$ has the form

$$\boldsymbol{d}_n = \begin{bmatrix} a & -b & 0\ldots & & \\ -b & a & -b & 0\ldots & \\ \vdots & & & \ddots & \\ & \ldots 0 & -b & a & -b \\ & & \ldots 0 & -b & a \end{bmatrix}, \tag{A.4}$$

where $0 < 2b < a$ then $|\, \boldsymbol{d}_n \,| > 0$ for all n, and

$$|\, \boldsymbol{d}_n \,| = a\,|\, \boldsymbol{d}_{n-1} \,| - b^2\,|\, \boldsymbol{d}_{n-2} \,|\,. \tag{A.5}$$

Let us denote

$$r_n = |\, \boldsymbol{d}_n \,| \,/\, |\, \boldsymbol{d}_{n-1} \,|\,. \tag{A.6}$$

Then from (A.5),

$$r_n = a - b^2/r_{n-1}. \tag{A.7}$$

Since $r_n > 0$ for all n, r_n is increasing and $r_n < a$ for all n. Therefore there exists the limit

$$L = \lim_{n\to\infty} r_n, \tag{A.8}$$

and $L \geqslant 0$. From (A.7) we necessarily have

$$L = a - b^2/L. \tag{A.9}$$

Substituting the relevant values of a and b we get

$$L = 4 - 2S - S^2/L. \tag{A.10}$$

This yields a quadratic equation for L. Solving it and taking the relevant root (with the plus sign) we get

$$L = 2 - S + 2\cos\theta. \tag{A.11}$$

Now, from (A.3),(A.10) and (A.11) we get

$$\lim_{P\to\infty}\eta_P^{(1)} = \frac{2S}{4-S-S^2/L} = \frac{2S}{S+4-2S-S^2/L} = \frac{2S}{S+L} = \frac{2S}{S+2-S+2\cos\theta} = \frac{S}{1+\cos\theta}$$
$$= \frac{1-\cos^2\theta}{1+\cos\theta} = 1-\cos\theta. \tag{A.12}$$

This proves (60), which means that the ABC truncation error approaches zero as P tends to infinity.

References

[1] T. Hagstrom, Radiation boundary conditions for the numerical simulation of waves, Acta Numer. 8 (1999) 47–106.
[2] J.P. Bérenger, A perfectly matched layer for the absorption of electromagnetic waves, J. Comput. Phys 114 (1994) 185–200.
[3] D. Appelo, T. Hagstrom, G. Kreiss, Perfectly matched layers for hyperbolic systems: general formulation, well-posedness, and stability, SIAM J. Appl. Math. 67 (2006) 1–23.
[4] D. Givoli, Non-reflecting boundary conditions: a review, J. Comput. Phys 94 (1991) 1–29.
[5] F. Collino, High order absorbing boundary conditions for wave propagation models. straight line boundary and corner cases, in: R. Kleinman et al. (Eds.), Proceedings of the 2nd International Conference on Mathematical & Numerical Aspects of Wave Propagation, SIAM, Delaware, 1993, pp. 161–171.
[6] D. Givoli, High-order local non-reflecting boundary conditions: a review, Wave Motion 39 (2004) 319–326.
[7] B. Engquist, A. Majda, Radiation boundary conditions for acoustic and elastic calculations, Commun. Pure Appl. Math. 32 (1979) 313–357.
[8] A. Bayliss, E. Turkel, Radiation boundary conditions for wave-like equations, Commun. Pure Appl. Math. 33 (1980) 707–725.
[9] R.L. Higdon, Numerical absorbing boundary conditions for the wave equation, Math. Comput. 49 (1987) 65–90.
[10] R.L. Higdon, Radiation boundary conditions for dispersive waves, SIAM J. Numer. Anal. 31 (1994) 64–100.
[11] D. Givoli, B. Neta, High-order non-reflecting boundary conditions for dispersive waves, Wave Motion 37 (2003) 257–271.
[12] G.J. Fix, S.P. Marin, Variational methods for underwater acoustic problems, J. Comp. Phys. 28 (1978) 253–270.
[13] D. Givoli, Recent advances in the DtN FE method, Arch. Comput. Meth. Eng. 6 (1999) 71–116.
[14] B. Alpert, L. Greengard, T. Hagstrom, Rapid evaluation of nonreflecting boundary kernels for time-domain wave propagation, SIAM J. Numer. Anal. 37 (2000) 1138–1164.
[15] T. Hagstrom, On high-order radiation boundary conditions, in: B. Engquist, G. Kriegsmann (Eds.), Computational Wave Propagation, Springer, 1997, pp. 1–22.
[16] T. Hagstrom, S.I. Hariharan, A formulation of asymptotic and exact boundary conditions using local operators, Appl. Numer. math. 27 (1998) 403–416.
[17] D. Givoli, B. Neta, High-order non-reflecting boundary scheme for time-dependent waves, J. Comput. Phys 186 (2003) 24–46.
[18] D. Givoli, B. Neta, I. Patlashenko, Finite element solution of exterior time-dependent wave problems with high-order boundary treatment, Int. J. Numer. Meth. Engng 58 (2003) 1955–1983.
[19] T. Hagstrom, T. Warburton, A new auxiliary variable formulation of high-order local radiation boundary conditions: corner compatibility conditions and extensions to first order systems, Wave Motion 39 (2004) 327–338.
[20] D. Givoli, T. Hagstrom, I. Patlashenko, Finite element formulation with high order absorbing boundary conditions for time-dependent waves, Comput. Meth. Appl. Mech. Eng. 195 (2006) 3666–3690.
[21] T. Hagstrom, M. de Castro, D. Givoli, D. Tzemach, Local high order absorbing boundary conditions for time-dependent waves in guides, J. Comput. Acoust. 15 (2007) 1–22.
[22] A. Taflove, S. Hagness, Computational Electrodynamics: The Finite-Difference Time-Domain Method, 2nd ed., Artech House, Boston, MA, 2000.
[23] J. Diaz, P. Joly, An analysis of higher order boundary conditions for the wave equation, SIAM J. Appl. Math. 65 (2005) 1547–1575.
[24] A. Taflove, Computational Electrodynamics: The Finite-Difference Time-Domain Method, Artech House, Boston MA, 1995.
[25] S. Asvadurov, V. Druskin, M. Guddati, L. Knizherman, On optimal finite difference approximation of PML, SIAM J. Numer. Anal. 41 (2003) 287–305.
[26] J. Diaz, P. Joly, A time-domain analysis of PML models in acoustics, Comput. Meth. Appl. Mech. Eng. 195 (2006) 3820–3853.
[27] T. Hagstrom, T. Warburton, Complete radiation boundary conditions: minimizing the long time error growth of local methods, submitted for publication.
[28] T. Hagstrom, T. Warburton, D. Givoli, Radiation boundary conditions for time-dependent waves based on complete plane wave expansions, submitted for publication.
[29] M. de Castro, Stability of parabolic systems on a half-space and theoretical aspects of absorbing boundary conditions, Doctoral Dissertation, The University of New Mexico, Albuquerque, NM, 2006.
[30] J. Pedlosky, Geophysical Fluid Dynamics, Springer, New York, 1987.
[31] A.D. Pierce, Acoustics, Acoustical Society of America, NY, 1989.
[32] T.J.R. Hughes, The Finite Element Method, Prentice Hall, Englewood Cliffs, NJ, 1987.
[33] L. Greengard, J. Huang, V. Rokhlin, S. Wandzura, Accelerating fast multipole methods for low frequency scattering, IEEE Comput. Sci. Eng. 5 (1998) 32–38.

[34] N. Yarvin, V. Rokhlin, Generalized gaussian quadratures and singular value decompositions of integral operators, SIAM J. Sci. Comput. 20 (1999) 699–718.
[35] B. Gustafsson, H.-O. Kreiss, J. Oliger, Time dependent problems and difference methods, Wiley, NY, 1995.
[36] T. Hagstrom, G. Hagstrom, Grid stabilization of high-order one-sided differencing I: First order hyperbolic systems, J. Comput. Phys. 223 (2007) 316–340.
[37] T. Hagstrom, G. Hagstrom, Grid stabilization of high-order one-sided differencing II: Second order wave equations, submitted for publication.
[38] A. Mar-Or, D. Givoli, The global–regional model interaction problem – analysis of carpenter's scheme and related issues, Int. J. Multiscale Comput. Eng. 4 (2006) 617–646.